ATLAS CONF Note

ATLAS-CONF-2017-030

8th May 2017

Search for supersymmetry in final states with two same-sign or three leptons and jets using 36 fb^{-1} of $\sqrt{s}$ = 13 TeV pp collision data with the ATLAS detector

The ATLAS Collaboration

A search for strongly produced supersymmetric particles using signatures involving several energetic jets and either two isolated same-sign leptons (e or μ), or at least three isolated leptons, is presented. The analysis relies on b-tagged jets and missing transverse momentum, to achieve good sensitivity. A data sample of proton–proton collisions at $\sqrt{s}$ = 13 TeV recorded with the ATLAS detector at the Large Hadron Collider in 2015 and 2016, corresponding to a total integrated luminosity of 36.1 fb^{-1}, is used for the search. No significant excess over the Standard Model expectation is observed. The results are interpreted in several simplified supersymmetric models featuring R-parity conservation and R-parity violation, extending the exclusion limits from previous searches. In models considering gluino pair production, gluino masses are excluded up to 1.85 TeV at 95% confidence level. When bottom squarks are pair-produced and decay to $t\tilde{\chi}_1^{\pm}$, models with bottom squark masses below 700 GeV and light neutralinos are excluded at 95% confidence level. In addition, model independent limits are set on a possible contribution of new phenomena to the signal region yields.

ATLAS-CONF-2017-030
09 May 2017

1 Introduction

Supersymmetry (SUSY) [1–6] is one of the most popular extensions of the Standard Model (SM). A general review can be found in Ref. [7]. In its minimal realisation (the MSSM) [8, 9] it predicts a new bosonic (fermionic) partner for each fundamental SM fermion (boson), as well as an additional Higgs doublet. If R-parity [10] is conserved (RPC) the lightest supersymmetric particle (LSP) is stable and can be the lightest neutralino[1] $\tilde{\chi}_1^0$. In many models, the LSP can be a dark matter candidate [11, 12] and produce signatures with large missing transverse momentum. On the contrary, if R-parity is violated (RPV), the LSP decay generates events with high jet and lepton multiplicity. Both RPC and RPV scenarios can produce the final state signature considered in this note.

In order to address the SM hierarchy problem with SUSY models [13–16], TeV-scale masses are required [17, 18] for the partners of the gluons (gluinos $\tilde{g}$) and of the top quarks (top squarks $\tilde{t}_\mathrm{L}$ and $\tilde{t}_\mathrm{R}$), due to the large top Yukawa coupling.[2] The latter also favours significant $\tilde{t}_\mathrm{L}$–$\tilde{t}_\mathrm{R}$ mixing, so that the mass eigenstate $\tilde{t}_1$ is lighter than all the other squarks in many scenarios [19, 20]. Bottom squarks ($\tilde{b}$) may also be light, being bound to top squarks by $SU(2)_\mathrm{L}$ invariance. This leads to potentially large production cross-sections for gluino pairs ($\tilde{g}\tilde{g}$), top–antitop squark pairs ($\tilde{t}_1\tilde{t}_1^*$) and bottom–antibottom squark pairs ($\tilde{b}_1\tilde{b}_1^*$) at the Large Hadron Collider (LHC) [21]. Production of isolated leptons may arise in the cascade decays of those superpartners to SM quarks and neutralinos $\tilde{\chi}_1^0$, via intermediate neutralinos $\tilde{\chi}_{2,3,4}^0$ or charginos $\tilde{\chi}_{1,2}^\pm$ that in turn lead to W, Z or Higgs bosons, or to lepton superpartners (sleptons, $\tilde{l}$). Light third-generation squarks would also enhance gluino decays to top or bottom quarks over the generic decays involving light-flavour squarks, favouring the production of heavy flavour quarks and, in the case of top quarks, additional isolated leptons.

This note presents a search for SUSY in final states with two leptons (electrons or muons) of the same electric charge, referred to as same-sign (SS) leptons or three leptons (3L), jets and in some cases also missing transverse momentum, whose magnitude is referred to as $E_\mathrm{T}^\mathrm{miss}$. It is an extension of an earlier search performed by the ATLAS experiment [22] with $\sqrt{s} = 13$ TeV data [23], and uses the data collected in proton–proton (pp) collisions during 2015 and 2016. Similar searches for SUSY in this topology were also performed by the CMS experiment at $\sqrt{s} = 13$ TeV [24–26]. While the same-sign or three lepton signatures are present in many scenarios of physics beyond the SM (BSM), SM processes leading to such final states have very small cross-sections. Compared to other BSM searches, analyses based on these signatures therefore allow the use of looser kinematic requirements (for example, on $E_\mathrm{T}^\mathrm{miss}$ or on the momentum of jets and leptons), preserving sensitivity to scenarios with small mass differences between the produced gluinos/squarks and the LSP, or in which R-parity is not conserved. This sensitivity to a wide range of BSM physics processes is illustrated by the interpretation of the results in the context of twelve different SUSY simplified models [27–29] that may lead to same-sign or three-lepton signatures.

For RPC models, the first four scenarios studied focus on gluino pair production with decays into on-shell (Fig. 1(a)) or off-shell (Fig. 1(b)) top quarks, as well as on-shell light quarks. The latter are accompanied by a cascade decay involving a $\tilde{\chi}_1^\pm$ and a $\tilde{\chi}_2^0$ (Fig. 1(c)) or a $\tilde{\chi}_2^0$ and light sleptons (Fig. 1(d)). The other two RPC scenarios target the direct production of third generation squark pairs with subsequent electroweakino-mediated decays (Fig. 1(e) and 1(f)). The former is characterized by final states with

[1] The SUSY partners of the Higgs and electroweak gauge bosons, the electroweakinos, mix to form the mass eigenstates known as charginos ($\tilde{\chi}_l^\pm$, $l = 1, 2$ ordered by increasing mass) and neutralinos ($\tilde{\chi}_m^0$, $m = 1, \ldots, 4$ ordered by increasing mass).

[2] The partners of the left-handed (right-handed) quarks are labelled $\tilde{q}_\mathrm{L(R)}$. In the case where there is significant L/R mixing (as is the case for third generation squarks) the mass eigenstates of these squarks are labelled $\tilde{q}_{1,2}$ ordered by increasing mass.

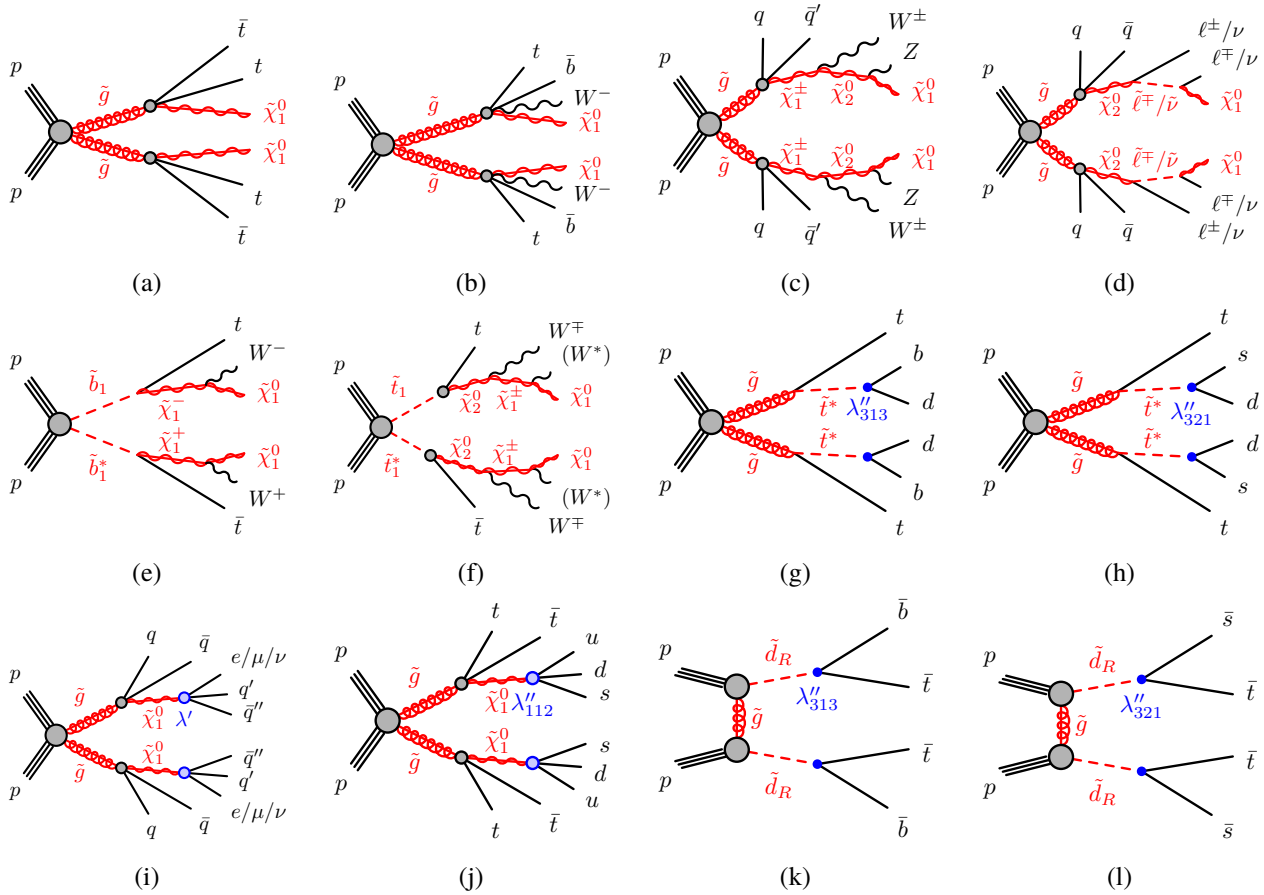

Figure 1: RPC SUSY processes featuring gluino ((a), (b), (c), (d)) or third generation squark ((e), (f)) pair production studied in this analysis. RPV SUSY models considered are gluino pair production ((g), (h), (i), (j)) and t-channel production of down squark-rights ((k), (l)) which decay via baryon or lepton number violating couplings λ'' and λ' respectively. In the diagrams, $q = u, d, c, s$ and $\ell = e, \mu, \tau$. In Figure 1(d), $\tilde{l} = \tilde{e}, \tilde{\mu}, \tilde{\tau}$ and $\tilde{\nu} = \tilde{\nu}_e, \tilde{\nu}_\mu, \tilde{\nu}_\tau$. In Figure 1(f), (W^*) indicates that W-boson is off-shell – the mass difference between $\tilde{\chi}_1^\pm$ and $\tilde{\chi}_1^0$ is around 1 GeV.

bottom squark pairs decaying to $t\bar{t}WW\tilde{\chi}_1^0\tilde{\chi}_1^0$. The latter, addressed here by looking for a three same-sign lepton final state, is a model that could explain the excess seen in same-sign lepton signatures during Run 1 [30]. Finally, a full SUSY model with low fine-tuning, the non-universal Higgs model with two extra parameters (NUHM2) [31, 32], is also considered. When the soft SUSY breaking electroweakino mass, $m_{1/2}$, is in the range 300–800 GeV, the model predominantly involves gluino pair production with gluinos decaying predominantely to $t\bar{t}\tilde{\chi}_1^0$ and $tb\tilde{\chi}_1^\pm$, giving rise to final states with two same-sign leptons and $E_{\mathrm{T}}^{\mathrm{miss}}$.

In the case of non-zero RPV couplings in the baryonic sector (λ''_{ijk}), as proposed in minimal flavour violation scenarios [33–35], gluinos and squarks may decay directly to top quarks, leading to final states with same-sign leptons [36, 37] and b-quarks (Figs. 1(g) and 1(h)). Although these figures illustrate decay modes mediated by non-zero λ''_{313} (resp. λ''_{321}) couplings, the exclusion limits set for these scenarios also hold for non-zero λ''_{323} (resp. λ''_{311} or λ''_{322}), as these couplings lead to experimentally undistinguishable final states. Alternatively a gluino decaying to a neutralino LSP, that further decays to SM particles via a non-zero RPV coupling in the leptonic sector, λ', or λ'', is also possible (Figs. 1(i) and 1(j)). Lower $E_{\mathrm{T}}^{\mathrm{miss}}$

is expected in these scenarios, as there is no stable LSP, and the $E_{\mathrm{T}}^{\mathrm{miss}}$ originates from neutrinos produced in the $\tilde{\chi}_1^0$ and top-quark decays. Pair-production of [3] same-sign down squark-rights (Figs. 1(k) and 1(l)) is also considered. In all of these scenarios, anti-squarks decay into the charge-conjugate final states of thoset indicated for the corresponding squarks, and gluinos decay with equal probabilities into the given final state or its charge conjugate.

2 ATLAS detector

The ATLAS experiment [22] is a multi-purpose particle detector with a forward-backward symmetric cylindrical geometry and nearly 4π coverage in solid angle.[4] The interaction point is surrounded by an inner detector (ID), a calorimeter system, and a muon spectrometer (MS). The ID provides precision tracking of charged particles with pseudorapidities $|\eta| < 2.5$ and is surrounded by a superconducting solenoid providing a 2 T axial magnetic field. It consists of pixel and silicon-microstrip detectors inside a transition radiation tracker. One significant upgrade for the $\sqrt{s} = 13$ TeV running period is the presence of the Insertable B-Layer [38], an additional pixel layer close to the interaction point, which provides high-resolution hits at small radius to improve the tracking and vertexing performance. In the pseudorapidity region $|\eta| < 2.5$, high-granularity lead/liquid-argon electromagnetic sampling calorimeters are used. A steel/scintillator tile calorimeter measures hadron energies for $|\eta| < 1.7$. The endcap and forward regions, spanning $1.5 < |\eta| < 4.9$, are instrumented with liquid-argon calorimeters for both the electromagnetic and hadronic measurements. The MS consists of three large superconducting toroids with eight coils each, a system of trigger and precision-tracking chambers, which provide triggering and tracking capabilities in the ranges $|\eta| < 2.4$ and $|\eta| < 2.7$, respectively. A two-level trigger system is used to select events [39]. The first-level trigger is implemented in hardware. This is followed by the software-based high-level trigger stage, which can run offline-like reconstruction, reducing the event rate to about 1 kHz.

3 Dataset and simulated event samples

The data used in this analysis were collected during 2015 and 2016 with a peak instantaneous luminosity of $L = 1.4 \times 10^{34}$ cm^{-2}s^{-1}. The mean number of pp interactions per bunch crossing (pile-up) in the dataset is 24. After the application of beam, detector and data quality requirements, the integrated luminosity considered corresponds to 36.1 fb^{-1}. The uncertainty on the combined 2015+2016 integrated luminosity is 3.2%. It is derived, following a methodology similar to that detailed in Ref. [40], from a preliminary calibration of the luminosity scale using x-y beam-separation scans performed in August 2015 and May 2016.

Monte Carlo (MC) simulated event samples are used to model the SUSY signals and to estimate the irreducible SM background with two same-sign and/or three "prompt" leptons (originating from on-shell

[3] These RPV baryon-number-violating couplings only apply to $SU(2)$ singlets.

[4] ATLAS uses a right-handed coordinate system with its origin at the nominal interaction point (IP) in the centre of the detector and the z-axis along the beam pipe. The x-axis points from the IP to the centre of the LHC ring, and the y-axis points upward. Cylindrical coordinates (r, ϕ) are used in the transverse plane, ϕ being the azimuthal angle around the beam pipe. The pseudorapidity is defined in terms of the polar angle θ as $\eta = -\ln\tan(\theta/2)$. Rapidity is defined as $y = 0.5 \ln[(E + p_z)/(E - p_z)]$ where E denotes the energy and p_z is the component of the momentum along the beam direction. The transverse momentum p_{T}, the transverse energy E_{T} and the missing transverse momentum $E_{\mathrm{T}}^{\mathrm{miss}}$ are defined in the $x - y$ plane.

heavy boson decays). The reducible background, mainly arising from $t\bar{t}$ production, is estimated from the data as described in Section 5.1. The MC samples are processed through a detailed ATLAS detector simulation [41] based on GEANT4 [42] or a fast simulation using a parameterization of the calorimeter response and GEANT4 for the ID and MS [43]. To simulate the effects of additional pp collisions in the same and nearby bunch crossings, inelastic interactions are generated using the soft strong interaction processes of PYTHIA 8.186 [44] with the A2 tune [45] and the MSTW2008LO parton distribution function (PDF) [46]. These MC events are overlaid onto the simulated hard scatter event and reweighted to match the pile-up conditions observed in the data. The event generator, parton shower, cross-section normalization, PDF set and underlying-event tune of all samples are presented in Table 1. In all MC samples, except those produced by the SHERPA generator, the EVTGEN v1.2.0 program [47] is used to model the properties of bottom and charm hadron decays.

Physics process	Event generator	Parton shower	Cross-section normalization	PDF set	Tune
Signal					
RPC	MG5_aMC@NLO 2.2.3 [48]	PYTHIA 8.186 [44]	NLO+NLL	NNPDF2.3LO [49]	A14 [50]
RPV except Fig. 1(j)	MG5_aMC@NLO 2.2.3	PYTHIA 8.210	or	NNPDF2.3LO	A14
RPV Fig. 1(j)	HERWIG 2.7.1 [51]	HERWIG 2.7.1	NLO-Prospino2 [52–57]	CTEQ6L1 [58]	UEEE5 [59]
$t\bar{t}+X$					
$t\bar{t}W, t\bar{t}Z/\gamma^*$	MG5_aMC@NLO 2.2.2	PYTHIA 8.186	NLO [60]	NNPDF2.3LO	A14
$t\bar{t}H$	MG5_aMC@NLO 2.3.2	PYTHIA 8.186	NLO [60]	NNPDF2.3LO	A14
$t\bar{t}t\bar{t}$ ($4t$)	MG5_aMC@NLO 2.2.2	PYTHIA 8.186	NLO [48]	NNPDF2.3LO	A14
Diboson					
ZZ, WZ	SHERPA 2.2.1 [61]	SHERPA 2.2.1	NLO [62]	NNPDF2.3LO	SHERPA default
Other (inc. $W^{\pm}W^{\pm}$)	SHERPA 2.1.1	SHERPA 2.1.1	NLO [62]	CT10 [63]	SHERPA default
Rare					
$t\bar{t}WW, t\bar{t}WZ$	MG5_aMC@NLO 2.2.2	PYTHIA 8.186	NLO [48]	NNPDF2.3LO	A14
$tZ, tWZ, tt\bar{t}$	MG5_aMC@NLO 2.2.2	PYTHIA 8.186	LO	NNPDF2.3LO	A14
WH, ZH	MG5_aMC@NLO 2.2.2	PYTHIA 8.186	NLO [64]	NNPDF2.3LO	A14
Triboson	SHERPA 2.1.1	SHERPA 2.1.1	NLO [62]	CT10	SHERPA default

Table 1: Simulated signal and background event samples: the corresponding event generator, parton shower, cross-section normalization, PDF set and underlying-event tune is shown for each sample. Because of their very small contribution to the signal region background estimate $t\bar{t}WW$, $t\bar{t}WZ$, tZ, tWZ, $tt\bar{t}$, WH, ZH and triboson are summed and labelled "Rare" in the following. NLO-Prospino2 refers to RPV down squark models of Fig.1(k) and 1(l), as well as the NUHM2 model.

The SUSY signals from Figure 1 are defined by an effective Lagrangian describing the interactions of a small number of new particles [27–29]. All SUSY particles not included in the decay of the pair-produced squarks and gluinos are effectively decoupled. These simplified models assume one production process and one decay channel with a 100% branching fraction. They are generated from leading order (LO) matrix elements with up to two extra partons in the matrix element (only up to one for the $\tilde{g} \to q\bar{q}(\ell\ell/\nu\nu)\tilde{\chi}_1^0$ model) using MG5_aMC@NLO 2.2.3 [48] interfaced to Pythia 8.186 with the A14 tune [50] for the modelling of the parton shower, hadronization and underlying event. Jet–parton matching is realised following the CKKW-L prescription [65], with a matching scale set to one quarter of the pair-produced superpartner mass. All signal models are generated with prompt decays of the SUSY particles. Signal cross-sections are calculated at next-to-leading order (NLO) in the strong coupling constant, adding the resummation of soft-gluon emission at next-to-leading-logarithmic accuracy (NLO+NLL) [52–56], except for the RPV models of Fig.1(k) and Fig.1(l) and the NUHM2 model where NLO cross-sections are used [52, 66]. The nominal cross-sections and the uncertainties are taken from envelopes of cross-section predictions using different PDF sets and factorisation and renormalization scales, as described in Refs. [21, 57]. Typical pair production cross-sections are: 4.7 ± 1.2 fb for gluinos with a mass of 1.7 TeV, 28.3 ± 4.0 fb for bottom squarks with a mass of 800 GeV, and 15.0 ± 2.0 fb for down squark rights with a

mass of 800 GeV and a gluino mass of 2.0 TeV.

The two dominant irreducible background processes are $t\bar{t}V$ (with V being a W or Z/γ^* boson) and diboson production with four charged leptons ℓ,[5] three charged leptons and one neutrino, or two same-sign charged leptons and two neutrinos. The MC simulation samples for these are described in detail in Refs. [67] and [62], respectively. For diboson production, the matrix elements contain the doubly resonant diboson processes and all other diagrams with four or six electroweak vertices, such as $W^\pm W^\pm jj$, with one ($W^\pm W^\pm jj$) or two (WZ, ZZ) extra partons. NLO cross-sections for $t\bar{t}W$, $t\bar{t}Z/\gamma^*(\rightarrow \ell\ell)$[6] and leptonic diboson processes are respectively 600.8 fb [60], 123.7 fb and 6.0 pb [62]. The processes $t\bar{t}H$ and $t\bar{t}t\bar{t}$, with NLO cross-sections of 507.1 fb [60] and 9.2 fb [48] respectively, are also considered.

Other background processes with small cross-sections are grouped into a category labelled "Rare". This category contains $t\bar{t}WW$ and $t\bar{t}WZ$ events generated with no extra parton in the matrix element, tZ, tWZ, $tt\bar{t}$, WH and ZH as well as triboson (WWW, WWZ, WZZ and ZZZ) production with up to six charged leptons. The processes $WWZ \rightarrow 4\ell + 2\nu, 2\ell + 4\nu$, $WWW, WZZ \rightarrow 3\ell + 3\nu$ and $ZZZ \rightarrow 6\ell + 0\nu, 4\ell + 2\nu, 2\ell + 4\nu$ are generated at NLO with additional LO matrix elements for up to two extra partons.

4 Object reconstruction and selection

Candidate events are required to have a reconstructed vertex [69], with at least two associated tracks with $p_{\mathrm{T}} > 400$ MeV. The vertex with the largest Σp_{T}^2 of the associated tracks is chosen as the primary vertex of the event.

For the data-driven background estimations, two categories of electrons and muons are used: "candidate" and "signal" with the latter being a subset of the "candidate" leptons satisfying tighter selection criteria. Electron candidates are reconstructed from energy depositions in the electromagnetic calorimeter that have been matched to an ID track and are required to have $|\eta| < 2.47$, $p_{\mathrm{T}} > 10$ GeV, and to pass the "Loose" likelihood-based identification requirement [70]. Candidates within the transition region between the barrel and endcap electromagnetic calorimeters, $1.37 < |\eta| < 1.52$, are not considered. The track matched with the electron must have a significance of the transverse impact parameter with respect to the reconstructed primary vertex, d_0, of $|d_0|/\sigma(d_0) < 5$. Muon candidates are reconstructed in the region $|\eta| < 2.5$ from muon spectrometer tracks matching ID tracks. All muon candidates must have $p_{\mathrm{T}} > 10$ GeV and must pass the "Medium" identification requirements [71].

Jets are reconstructed with the anti-k_t algorithm [72] with radius parameter $R = 0.4$, using three-dimensional topological energy clusters in the calorimeter [73] as input. All jets must have $p_{\mathrm{T}} > 20$ GeV and $|\eta| < 2.8$. For all jets the expected average energy contribution from pile-up is subtracted according to the jet area [74, 75]. Jets are then calibrated as described in Ref. [75]. In order to reduce the effects of pile-up, jets with $p_{\mathrm{T}} < 60$ GeV and $|\eta| < 2.4$ are required to have a significant fraction of their associated tracks originating from the primary vertex, as defined by the jet vertex tagger (JVT) [76].

Identification of jets containing b-hadrons (b-tagging) is performed with the MV2c10 algorithm, a multivariate discriminant making use of track impact parameters and reconstructed secondary vertices [77, 78]. A requirement is chosen corresponding to a 70% average efficiency for tagging b-jets in simulated $t\bar{t}$

[5] All lepton flavours are included here and τ leptons subsequently decayed leptonically or hadronically.
[6] This cross-section is computed using the configuration of Refs. [48, 68].

events. The rejection factors for light-quark/gluon jets, c-quark jets and hadronically decaying τ leptons in simulated $t\bar{t}$ events are approximately 380, 12 and 54, respectively [78, 79]. Jets with $|\eta| < 2.5$ which satisfy the b-tagging and JVT requirements are identified as b-jets. Correction factors and uncertainties determined from data for the b-tagging efficiencies and mis-tag rates are applied to the simulated samples [78].

After the object identification, overlaps between the different objects are resolved. Any jet within a distance $\Delta R_y = \sqrt{(\Delta y)^2 + (\Delta\phi)^2} = 0.2$ of a lepton candidate is discarded, unless the jet is b-tagged[7], in which case the lepton is discarded since it is likely originating from a semileptonic b-hadron decay. Any remaining lepton within $\Delta R_y = \min\{0.4, 0.1 + 9.6\,\text{GeV}/p_{\text{T}}(\ell)\}$ of a jet is discarded. In the case of muons, the muon is retained and the jet is discarded if the jet has fewer than three associated tracks. This recovers inefficiencies for high-energy muons undergoing significant energy loss in the calorimeter.

Signal electrons must satisfy the "Medium" likelihood-based identification requirement [70]. In regions with large amounts of material in the tracker, an electron (resp. positron) may more likely emit a hard bremsstrahlung photon. If the photon subsequently converts to an asymmetric electron–positron pair, and the the positron (resp. electron) is high momentum and reconstructed, the lepton charge can be mis-identified (later referred to as "charge-flip"). To reduce the impact of charge mis-identification, signal electrons must satisfy $|\eta| < 2.0$. Furthermore, signal electrons that are likely to be reconstructed with an incorrect charge assignment are rejected using the following electron cluster and track properties including the impact parameter, the curvature significance, the cluster width, and the quality of the matching between the cluster and its associated track, both in terms of energy and position. These variables, as well as the electron p_{T} and η, are combined into a single classifier using a boosted decision tree (BDT) algorithm. A selection requirement on the BDT output is chosen to achieve a rejection factor between 7 and 8 for electrons with a wrong charge assignment while selecting correctly measured electrons with an efficiency of 97%. Correction factors to account for differences in the selection efficiency between data and MC simulation have been applied to the selected electrons in the MC simulation. These correction factors are determined using $Z \to ee$ events [80].

Signal muons must fulfil the requirement $|d_0|/\sigma(d_0) < 3$. Tracks associated with the signal electrons or muons must have a longitudinal impact parameter with respect to the reconstructed primary vertex, z_0, satisfying $|z_0 \sin\theta| < 0.5$ mm. Isolation requirements are applied to both the signal electrons and muons. The scalar sum of the p_{T} of tracks within a variable-size cone around the lepton, excluding its own track, must be less than 6% of the lepton p_{T}. The track isolation cone radius for electrons (muons) $\Delta R_\eta = \sqrt{(\Delta\eta)^2 + (\Delta\phi)^2}$ is given by the smaller of $\Delta R_\eta = 10\ \text{GeV}/p_{\text{T}}$ and $\Delta R_\eta = 0.2\,(0.3)$. In addition, in the case of electrons the calorimeter energy clusters in a cone of $\Delta R_\eta = 0.2$ around the electron (excluding the deposit from the electron itself) must be less than 6% of the electron p_{T}. Simulated events are corrected to account for differences in the lepton trigger, reconstruction, identification and isolation efficiencies between data and MC simulation.

The missing transverse momentum is defined as the negative vector sum of the transverse momenta of all identified candidate objects (electrons, photons [81], muons and jets) and an additional soft term. The soft term is constructed from all tracks that are not associated with any physics object, but are associated with the primary vertex. In this way, the $E_{\text{T}}^{\text{miss}}$ is adjusted for the best calibration of the jets and the other identified physics objects above, while maintaining approximate pile-up independence in the soft term [82, 83].

[7] In this case the b-tagging operating point corresponding to an efficiency of 85% is used.

Events are selected using a combination of dilepton and $E_{\mathrm{T}}^{\mathrm{miss}}$ triggers, the latter being used only for events with $E_{\mathrm{T}}^{\mathrm{miss}} > 250\,\mathrm{GeV}$. The trigger-level requirements on $E_{\mathrm{T}}^{\mathrm{miss}}$ and the leading and subleading lepton p_{T} are looser than those applied offline to ensure that trigger efficiencies are constant in the relevant phase space. The event selection requires at least two signal leptons with $p_{\mathrm{T}} > 20$ GeV (apart from two SRs where the subleading lepton p_{T} should be greater than 10 GeV[8]). If the event contains exactly two signal leptons, they must have the same electric charge. Events are discarded if they contain any jet failing basic quality selection criteria in order to reject detector noise and non-collision background events [84, 85].

To maximize the sensitivity to the signal models of Figure 1, nineteen mutually non-exclusive signal regions are defined in Table 2. The SRs are named in the form *SNLMbX*, where *S* indicates if the SR is targeting an RPC or RPV model, *N* indicates the number of leptons required, *M* the number of *b*-jets required, and *X* indicates the severity of the $E_{\mathrm{T}}^{\mathrm{miss}}$ or m_{eff} requirements (Soft, Medium or Hard). The requirements used to define the SRs are the number of signal leptons ($N_{\mathrm{leptons}}^{\mathrm{signal}}$), number of *b*-jets with $p_{\mathrm{T}} > 20\,\mathrm{GeV}$ ($N_{b\text{-jets}}$), number of jets with p_{T} above 25, 40 or 50 GeV, regardless of their flavour (N_{jets}), $E_{\mathrm{T}}^{\mathrm{miss}}$, the effective mass ($m_{\mathrm{eff}}$) and the charge of the signal leptons. The m_{eff} variable is defined as the scalar sum of the p_{T} of the signal leptons, jets and the $E_{\mathrm{T}}^{\mathrm{miss}}$. For SRs where the Z+jets background is important (Rpc3LSS1b, Rpv2L0b and Rpv2L2bH), events with a two same-sign electron invariant mass close to the Z-boson mass are vetoed. For SRs targeting the production of down squark pairs (Rpv2L1bS, Rpv2L2bS, Rpv2L1bM), only events with at least two negatively-charged leptons are considered, as the down squarks decay exclusively to top anti-quarks. Finally, SRs targeting signal scenarios with lepton p_{T} spectra softer than typical background processes impose an upper cut on the leptons' p_{T}. The last column indicates the targeted signal model. The Rpc3L1b and Rpc3L1bH SRs are not motivated by a particular signal model and can be seen as a natural extension of the Rpc3L0b SRs with the same kinematic cuts but requiring at least one *b*-jet.

The values of acceptance times efficiency of the SR selections for the RPC SUSY signal models, with masses near the exclusion limit, typically range between 0.5% and 7% for models with a light $\tilde{\chi}_1^0$ and 0.5–2% for models with a heavy $\tilde{\chi}_1^0$. For RPV SUSY signal models, these values are in the range 0.2–4%. To increase the signal efficiency for the SUSY models with low energetic leptons (Figure 1(b) and 1(c)), the p_{T} threshold of leptons is relaxed from 20 to 10 GeV in the SR definition.

5 Background estimation

Two main sources of SM background can be distinguished in this analysis. The first category is the reducible background, which includes events containing electrons with mis-measured charge, mainly from the production of top-quark pairs, and events containing at least one fake or non-prompt (FNP) lepton. The FNP lepton mainly originates from heavy-flavour hadron decays in events containing top quarks, W or Z bosons. Hadrons mis-identified as leptons, electrons from photon conversions and leptons from pion or kaon decays in flight are other possible sources. Data-driven methods used for the estimation of this reducible background in the signal and validation regions are described in Section 5.1. The second category is the irreducible background from events with two same-sign prompt leptons or at least three prompt leptons and is estimated using the MC simulation samples. Since diboson and $t\bar{t}V$ events are the main backgrounds in the signal regions, dedicated validation regions (VR) with an enhanced contribution

[8] In order to ensure that the trigger efficiency is constant for selected events where the subleading lepton p_{T} lies between 10 and 20 GeV the $E_{\mathrm{T}}^{\mathrm{miss}}$ trigger is choosen.

Signal region	$N_{\text{leptons}}^{\text{signal}}$	$N_{b\text{-jets}}$	N_{jets}	$p_{\text{T}}^{\text{jet}}$ [GeV]	$E_{\text{T}}^{\text{miss}}$ [GeV]	m_{eff} [GeV]	$E_{\text{T}}^{\text{miss}}/m_{\text{eff}}$	Other	Targeted Signal
Rpc2L2bS	$\geq$ 2SS	≥ 2	≥ 6	> 25	> 200	> 600	> 0.25	–	Fig. 1(a)
Rpc2L2bH	$\geq$ 2SS	≥ 2	≥ 6	> 25	–	> 1800	> 0.15	–	Fig. 1(a), NUHM2
Rpc2Lsoft1b	$\geq$ 2SS	≥ 1	≥ 6	> 25	> 100	–	> 0.3	20,10 $< p_{\text{T}}^{\ell_1}, p_{\text{T}}^{\ell_2} <$ 100 GeV	Fig. 1(b)
Rpc2Lsoft2b	$\geq$ 2SS	≥ 2	≥ 6	> 25	> 200	> 600	> 0.25	20,10 $< p_{\text{T}}^{\ell_1}, p_{\text{T}}^{\ell_2} <$ 100 GeV	Fig. 1(b)
Rpc2L0bS	$\geq$ 2SS	$= 0$	≥ 6	> 25	> 150	–	> 0.25	–	Fig. 1(c)
Rpc2L0bH	$\geq$ 2SS	$= 0$	≥ 6	> 40	> 250	> 900	–	–	Fig. 1(c)
Rpc3L0bS	≥ 3	$= 0$	≥ 4	> 40	> 200	> 600	–	–	Fig. 1(d)
Rpc3L0bH	≥ 3	$= 0$	≥ 4	> 40	> 200	> 1600	–	–	Fig. 1(d)
Rpc3L1bS	≥ 3	≥ 1	≥ 4	> 40	> 200	> 600	–	–	None
Rpc3L1bH	≥ 3	≥ 1	≥ 4	> 40	> 200	> 1600	–	–	None
Rpc2L1bS	$\geq$ 2SS	≥ 1	≥ 6	> 25	> 150	> 600	> 0.25	–	Fig. 1(e)
Rpc2L1bH	$\geq$ 2SS	≥ 1	≥ 6	> 25	> 250	–	> 0.2	–	Fig. 1(e)
Rpc3LSS1b	$\geq \ell^{\pm}\ell^{\pm}\ell^{\pm}$	≥ 1	–	–	–	–	-	veto 81$< m_{e^{\pm}e^{\pm}} <$101 GeV	Fig. 1(f)
Rpv2L1bH	$\geq$ 2SS	≥ 1	≥ 6	> 50	–	> 2200	–	–	Figs. 1(g),1(h)
Rpv2L0b	$=$ 2SS	$= 0$	≥ 6	> 40	–	> 1800	–	veto 81$< m_{e^{\pm}e^{\pm}} <$101 GeV	Fig. 1(i)
Rpv2L2bH	$\geq$ 2SS	≥ 2	≥ 6	> 40	–	> 2000	–	veto 81$< m_{e^{\pm}e^{\pm}} <$101 GeV	Fig. 1(j)
Rpv2L2bS	$\geq \ell^{-}\ell^{-}$	≥ 2	≥ 3	> 50	–	> 1200	–	–	Fig. 1(k)
Rpv2L1bS	$\geq \ell^{-}\ell^{-}$	≥ 1	≥ 4	> 50	–	> 1200	–	–	Fig. 1(l)
Rpv2L1bM	$\geq \ell^{-}\ell^{-}$	≥ 1	≥ 4	> 50	–	> 1800	–	–	Fig. 1(l)

Table 2: Summary of the signal region definitions. Unless explicitely stated in the table, at least two signal leptons with p_{T} >20 GeV and same charge (SS) are required in each signal region. Requirements are placed on the number of signal leptons ($N_{\text{leptons}}^{\text{signal}}$), the number of b-jets with $p_{\text{T}} > 20$ GeV ($N_{b\text{-jets}}$), the number of jets (N_{jets}) above a certain p_{T} thresholds ($p_{\text{T}}^{\text{jet}}$), $E_{\text{T}}^{\text{miss}}$, m_{eff} and/or $E_{\text{T}}^{\text{miss}}/m_{\text{eff}}$. The last column indicates the targeted signal model.

from these processes, and small signal contamination, are defined to verify the background predictions from the simulation (Section 5.2). Section 5.3 discusses the systematic uncertainties considered when performing the background estimation in the signal and validation regions.

5.1 Reducible background estimation methods

Charge mis-identification is only relevant for electrons. The contribution of charge-flip events to the SR/VR is estimated using the data. The electron charge-flip probability is extracted in a $Z/\gamma^* \to ee$ data sample using a likelihood fit which takes as input the numbers of same-sign and opposite-sign electron pairs observed in a window of 10 GeV around the Z boson mass. The charge-flip probability is a free parameter of the fit and is extracted as a function of the electron p_{T} and η. These probabilities are around 0.5% (1%) and 0.1% (0.2%) for the candidate and signal electrons for $|\eta| < 1.37 (|\eta| > 1.52)$, respectively. The former is used only in the FNP lepton background estimation. The event yield of the charge-flip electron background in the signal or validation regions is obtained by multiplying the measured charge-flip probability with the number of events in data regions with the same kinematic requirements as the signal or validation regions but with opposite-sign lepton pairs.

Two data-driven methods are used to estimate the FNP lepton background, referred to as the "matrix method" and the "MC template method". The estimates from these methods are combined to give the final estimate. These two methods are described below.

The first estimation of the FNP lepton background is performed with a matrix method similar to that described in Ref. [86]. Two types of lepton identification criteria are defined: "tight", corresponding to

the signal lepton criteria described in Section 4, and "loose", corresponding to candidate leptons after object overlap removal and the charge-flip BDT selection described also in Section 4. The matrix method relates the number of events containing prompt or FNP leptons to the number of observed events with tight or loose-not-tight leptons using the probability for loose prompt or FNP leptons to satisfy the tight criteria. The probability for loose prompt leptons to satisfy the tight selection criteria (ε) is obtained using a $Z/\gamma^* \to \ell\ell$ data sample and is modelled as a function of the lepton p_{T} and η. The efficiencies for electrons (muons) rise from 60% (80%) at low p_{T} to almost 100% at p_{T} above 50 GeV – apart from endcap electrons which reach only 95%. The probability for loose FNP leptons to satisfy the tight selection criteria (FNP lepton rate, f) is determined from data in SS control regions enriched in non-prompt leptons mostly originating from heavy-flavour hadron decays in single lepton $t\bar{t}$ events. This region contains events with at least one b-jet, one well-isolated muon (referred to as the "tag"), and an additional loose electron or muon which is used for the measurement. The rates f are measured as function of p_{T}[9] after subtracting the small contribution from prompt lepton processes predicted by simulation and the data-driven estimation of events with electron charge-flip. For electrons, and muons with $|\eta| < 2.3$, f is constant around 10% for $p_{\mathrm{T}} < 30$ GeV and increases at higher p_{T}. These values of ε and f correspond to a regime where the method has been demonstrated to correctly estimate the FNP lepton background.

The second method for FNP lepton estimation is the MC template method [86, 87]. It relies on the correct modelling of the kinematic distributions of the FNP leptons and charge-flipped electron processes in $t\bar{t}$ and V+jets samples. These samples are simulated with the Powheg-Box generator [88–91] and the parton shower and hadronization performed by either Pythia 6.428 [92] ($t\bar{t}$) or Pythia 8.186 (V+jets). The FNP leptons are classified in five categories, namely electrons and muons coming from b and light-quark jets as well as photon conversions. Normalization factors for each of the five sources are adjusted to match the observed data in dedicated control regions. Events are selected with at least two same-sign signal leptons, $E_{\mathrm{T}}^{\mathrm{miss}} > 40$ GeV, two or more jets, and are required to be orthogonal to the SRs. They are further split into regions with or without b-jets and with different lepton flavours of the same-sign lepton pair, giving a total of six control regions. The global normalization factors applied to the MC samples estimating the reducible background in each SR varies from 1.2 ± 1.1 to 2.9 ± 2.0, where the errors account for statistical uncertainties and uncertainties related to the choice of the event generator (see Section 5.3).

Since the FNP lepton predictions from the MC template and matrix methods in the signal and validation regions are consistent with each other, a weighted average of the two results is used. This approach implies that the combined estimate is dominated by systematic uncertainties, which is not always the case when the matrix method is used, due to limited statistics in the control regions. To check the validity and robustness of the FNP lepton estimate, the distributions of several discriminating variables in data are compared with the predicted background after various requirements on the number of jets and b-jets. Examples of such distributions are shown in Fig. 2, and illustrate that the data are described by the prediction within uncertainties. The apparent disagreement for m_{eff} above 1 TeV in Figure 2(d) is covered by the large theory uncertainty for the diboson background, which is not shown on the Figure but amounts to about 30% for m_{eff} above 1 TeV.

5.2 Validation of irreducible background estimates

Dedicated validation regions are defined to verify the estimate of the $t\bar{t}V$, WZ and $W^{\pm}W^{\pm}$ background in the signal regions. The corresponding selections are summarized in Table 3. The overlap with the signal

[9] For muons with $p_{\mathrm{T}} < 20$ GeV, f is parametrized as a function of p_{T} and η.

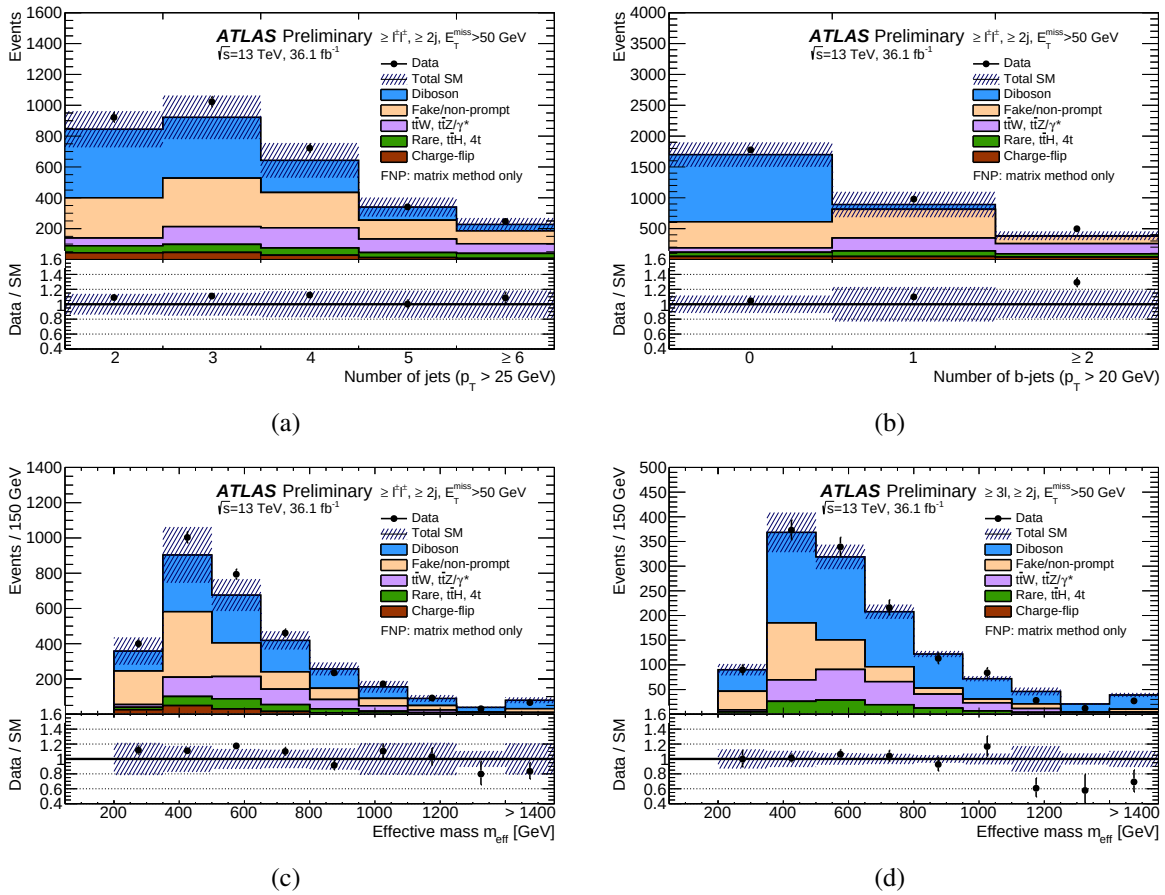

Figure 2: Distributions of the number of jets (a), of b-tagged jets (b) and of the effective mass ((c), (d)). The distributions are made after requiring at least two jets ($p_{\mathrm{T}} > 40\,\mathrm{GeV}$) and $E_{\mathrm{T}}^{\mathrm{miss}} > 50\,\mathrm{GeV}$, as well as at least two same-sign leptons ((a), (b), (c)) or three leptons (d). The uncertainty bands include the statistical uncertainties for the background prediction as well as the systematic uncertainties for fake or non-prompt lepton backgrounds (using the matrix method) and charge-flip electrons. Not included are theoretical uncertainties on the irreducible background contributions. The "rare" category is defined in the text.

regions is resolved by removing events that are selected in the signal regions. The purity of the targeted background processes in these regions ranges from about 35% to 65%. The expected signal contamination is generally below 5% for models near the limit of exclusion in $t\bar{t}Z$, WZ and $W^{\pm}W^{\pm}$ VRs and about 20% in the $t\bar{t}W$ VR. The observed yields, compared with the background predictions and uncertainties, can be seen in Table 4. There is good agreement between data and the estimated background in all the validation regions.

5.3 Systematic uncertainties

Statistical uncertainties due to the limited number of data events in the loose and tight lepton control regions are considered in the FNP lepton background estimate. In the matrix method, the systematic uncertainties mainly come from potentially different compositions of b-jets, light-quark jets and photon conversions between the control and the signal regions. The uncertainty coming from the prompt lepton

Validation Region	$N_{\text{leptons}}^{\text{signal}}$	$N_{b\text{-jets}}$	N_{jets}	$p_{\text{T}}^{\text{jet}}$ [GeV]	$E_{\text{T}}^{\text{miss}}$ [GeV]	m_{eff} [GeV]	Other
$t\bar{t}W$	$= 2SS$	≥ 1	≥ 4 ($e^{\pm}e^{\pm}$, $e^{\pm}\mu^{\pm}$) ≥ 3 ($\mu^{\pm}\mu^{\pm}$)	> 40 > 25	> 45	> 550	$p_{\text{T}}^{\ell_2} > 40$ GeV $\sum p_{\text{T}}^{b\text{-jet}} / \sum p_{\text{T}}^{\text{jet}} > 0.25$
$t\bar{t}Z$	≥ 3 ≥ 1 SFOS pair	≥ 1	≥ 3	> 35	–	> 450	$81 < m_{\text{SFOS}} < 101$ GeV
WZ4j	$= 3$	$= 0$	≥ 4	> 25	–	> 450	$E_{\text{T}}^{\text{miss}} / \sum p_{\text{T}}^{\ell} < 0.7$
WZ5j	$= 3$	$= 0$	≥ 5	> 25	–	> 450	$E_{\text{T}}^{\text{miss}} / \sum p_{\text{T}}^{\ell} < 0.7$
$W^{\pm}W^{\pm}jj$	$= 2SS$	$= 0$	≥ 2	> 50	> 55	> 650	veto $81 < m_{e^{\pm}e^{\pm}} < 101$ GeV $p_{\text{T}}^{\ell_2} > 30$ GeV $\Delta R_{\eta}(\ell_{1,2}, j) > 0.7$ $\Delta R_{\eta}(\ell_1, \ell_2) > 1.3$
All	Veto events belonging to any SR						

Table 3: Summary of the event selection in the validation regions (VRs). Requirements are placed on the number of signal leptons ($N_{\text{leptons}}^{\text{signal}}$), the number of b-jets with $p_{\text{T}} > 20$ GeV ($N_{b\text{-jets}}$) or the number of jets (N_{jets}) above a certain p_{T} threshold ($p_{\text{T}}^{\text{jet}}$). The two leading-$p_{\text{T}}$ leptons are referred to as $\ell_{1,2}$ with decreasing p_{T}. Additional requirements are set on $E_{\text{T}}^{\text{miss}}$, m_{eff}, the invariant mass of the two leading electrons $m_{e^{\pm}e^{\pm}}$, the presence of SS leptons or a pair of same-flavour opposite-sign leptons (SFOS) and its invariant mass m_{SFOS}. A minimum angular separation between the leptons and the jets ($\Delta R_{\eta}(\ell_{1,2}, j)$) and between the two leptons ($\Delta R_{\eta}(\ell_1, \ell_2)$) is imposed in the $W^{\pm}W^{\pm}jj$ VR. For the two WZ VRs an upper cut on the ratio between the $E_{\text{T}}^{\text{miss}}$ in the event and the sum of p_{T} of all signal leptons p_{T} ($E_{\text{T}}^{\text{miss}}/\sum p_{\text{T}}^{\ell}$) is required. An upper cut on the ratio between the scalar sum of the p_{T} of all b-jets and that of all jets in the event ($\sum p_{\text{T}}^{b\text{-jet}} / \sum p_{\text{T}}^{\text{jet}}$) is considered only in the $t\bar{t}W$ VR.

Validation Region	$t\bar{t}W$	$t\bar{t}Z$	WZ4j	WZ5j	$W^{\pm}W^{\pm}jj$
$t\bar{t}Z/\gamma^*$	6.2 ± 0.9	123 ± 17	17.8 ± 3.5	10.1 ± 2.3	1.06 ± 0.22
$t\bar{t}W$	19.0 ± 2.9	1.71 ± 0.27	1.30 ± 0.32	0.45 ± 0.14	4.1 ± 0.8
$t\bar{t}H$	5.8 ± 1.2	3.6 ± 1.8	1.8 ± 0.6	0.96 ± 0.34	0.69 ± 0.14
$t\bar{t}t\bar{t}$	1.02 ± 0.22	0.27 ± 0.14	0.04 ± 0.02	0.03 ± 0.02	0.03 ± 0.02
$W^{\pm}W^{\pm}$	0.5 ± 0.4	–	–	–	26 ± 14
WZ	1.4 ± 0.8	29 ± 17	200 ± 110	70 ± 40	27 ± 14
ZZ	0.04 ± 0.03	5.5 ± 3.1	22 ± 12	9 ± 5	0.53 ± 0.30
Rare	2.2 ± 0.5	26 ± 13	7.3 ± 2.1	3.0 ± 1.0	1.8 ± 0.5
Fake/non-prompt leptons	18 ± 16	22 ± 14	49 ± 31	17 ± 12	13 ± 10
Charge-flip	3.4 ± 0.5	–	–	–	1.74 ± 0.22
Total SM background	57 ± 16	212 ± 35	300 ± 130	110 ± 50	77 ± 31
Observed	71	209	257	106	99

Table 4: The number of observed data and expected background events in the validation regions. The "rare" category is defined in the text. Background categories shown as a "–" denote that they do not contribute to a given region (e.g. charge flips in 3-lepton regions) or that their estimates are below 0.01 events. The displayed yields include all sources of statistical and systematic uncertainties described in Section 5.3.

contamination in the FNP lepton control regions is also considered. Overall, the uncertainty on the FNP lepton rate f amounts to 30% at low p_{T}, and increases up to 85% for muons with $p_{\text{T}} > 40$ GeV and 50% for electrons with $p_{\text{T}} > 20$ GeV – the uncertainties on the real lepton efficiency ε are much lower.

The uncertainties on the FNP lepton estimation in each VRs and SRs are then evaluated by propagating f and ε uncertainties in the matrix method. In the MC template method, the systematic uncertainty is obtained by varying the generator from Powheg-Box to Sherpa and evaluating the impact on the global normalization scale factors applied to the MC samples. They are in the range 35–85%, depending on the SRs. The propagation of these uncertainties allows to obtain the uncertainties on the FNP lepton estimation in the SRs. When combining the results of the MC template and matrix methods to obtain the final estimate, systematic uncertainties are propagated assuming conservatively a full correlation between the two methods. When the FNP lepton estimate is below 0.15 events, the expected yield is set to 0.15 events with a 100% uncertainty.

The uncertainty in the electron charge-flip probability mainly originates from the limited number of events in the regions used in the charge-flip probability measurement and the uncertainty related to the background subtraction in the Z-boson mass peak. The relative error on the charge-flip rate is below 20% (30%) for signal (candidate) electrons with p_{T} above 20 GeV.

The systematic uncertainties related to the estimate of the same-sign prompt leptons background arise from the theoretical and experimental modelling in the MC simulation. The primary sources of systematic uncertainties are related to the experimental uncertainties (jet energy scale calibration, jet energy resolution, b-tagging efficiency) as well as theoretical modelling and theoretical cross-section uncertainties. The statistical uncertainty of the simulated event samples is also taken into account.

The cross-sections used to normalise the MC samples are varied according to the uncertainty in the cross-section calculation, which is 13% for $t\bar{t}W$, 12% for $t\bar{t}Z$ production [60], 6% for diboson production [62], 8% for $t\bar{t}H$ [60] and 30% for $t\bar{t}t\bar{t}$ [48]. Additional uncertainties are assigned to some of these backgrounds to account for the theoretical modelling of the kinematic distributions in the MC simulation. For $t\bar{t}W$ and $t\bar{t}Z$, the predictions from the MG5_aMC@NLO and Sherpa generators are compared, and the renormalization and factorisation scales used to generate these samples are varied independently within a factor of two, leading to a 15–35% uncertainty on the expected SR yields for these processes. For diboson production, uncertainties are estimated by varying the QCD and matching scales, as well as the parton shower recoil scheme, leading to a 30–40% uncertainty for these processes after the SR selections. For $t\bar{t}H$, $t\bar{t}t\bar{t}$ and rare production processes, a 50% uncertainty on their total contribution is assigned.

6 Results and interpretation

Figure 3(a) shows the event yields for data and the expected background contributions in all signal regions. Detailed information on the yields can be found in Table 5. In all 19 SRs the number of observed data events is consistent with the background expectation within the uncertainties. The contributions listed in the rare category are dominated by triboson, tWZ and $t\bar{t}WW$ production. The triboson processes generally dominate in the SRs with no b-jets, while tWZ and $t\bar{t}WW$ dominate in the SRs with one and two b-jets, respectively. WH, ZH, tZ and $t\bar{t}t$ production never constitute more than 20% of the rare background.

Figure 3(b) summarises the contributions of the different sources of systematic uncertainty on the total SM background predictions in the signal regions. The uncertainties amount to 25–45% of the total background depending on the signal region, dominated by systematics uncertainties coming from the reducible background or the theory.

In the absence of any significant deviation from the SM predictions, upper limits on possible BSM contributions to the signal regions are derived, as well as exclusion limits on the masses of SUSY particles

Signal Region	**Rpc2L2bS**	**Rpc2L2bH**	**Rpc2Lsoft1b**	**Rpc2Lsoft2b**	**Rpc2L0bS**	**Rpc2L0bH**
$t\bar{t}+W/Z\gamma^*$	1.6 ± 0.4	0.44 ± 0.14	1.3 ± 0.4	1.21 ± 0.33	0.82 ± 0.31	0.20 ± 0.10
$t\bar{t}H$	0.43 ± 0.25	0.10 ± 0.06	0.45 ± 0.24	0.36 ± 0.21	0.27 ± 0.15	0.08 ± 0.07
$t\bar{t}t\bar{t}$	0.26 ± 0.13	0.18 ± 0.09	0.09 ± 0.05	0.21 ± 0.11	0.01 ± 0.01	0.02 ± 0.02
Diboson	0.10 ± 0.10	0.04 ± 0.02	0.17 ± 0.09	0.05 ± 0.03	3.1 ± 1.4	1.0 ± 0.5
Rare	0.33 ± 0.18	0.15 ± 0.09	0.18 ± 0.10	0.17 ± 0.10	0.19 ± 0.11	0.17 ± 0.10
Fake/non-prompt leptons	0.5 ± 0.6	0.15 ± 0.15	3.5 ± 2.4	1.7 ± 1.5	1.6 ± 1.0	0.9 ± 0.9
Charge-flip	0.10 ± 0.01	0.02 ± 0.01	0.08 ± 0.02	0.08 ± 0.02	0.05 ± 0.01	0.01 ± 0.01
Total Background	3.3 ± 1.0	1.08 ± 0.32	5.8 ± 2.5	3.8 ± 1.6	6.0 ± 1.8	2.4 ± 1.0
Observed	3	0	4	5	7	3
S^{95}_{obs}	5.5	3.6	6.3	7.7	8.3	6.1
S^{95}_{exp}	$5.6^{+2.2}_{-1.5}$	$3.9^{+1.4}_{-0.4}$	$7.1^{+2.5}_{-1.5}$	$6.2^{+2.6}_{-1.5}$	$7.5^{+2.6}_{-1.8}$	$5.3^{+2.1}_{-1.3}$
σ_{vis} [fb]	0.15	0.10	0.17	0.21	0.23	0.17
p_0 (Z)	0.71 (–)	0.91 (–)	0.69 (–)	0.30 (0.5σ)	0.36 (0.4σ)	0.35 (0.4σ)

Signal Region	**Rpc3L0bS**	**Rpc3L0bH**	**Rpc3L1bS**	**Rpc3L1bH**	**Rpc2L1bS**	**Rpc2L1bH**	**Rpc3LSS1b**
$t\bar{t}+W/Z\gamma^*$	0.98 ± 0.25	0.18 ± 0.08	7.1 ± 1.1	1.54 ± 0.28	4.0 ± 1.0	4.0 ± 0.9	–
$t\bar{t}H$	0.12 ± 0.08	0.03 ± 0.02	1.4 ± 0.7	0.25 ± 0.14	1.3 ± 0.7	1.0 ± 0.6	0.22 ± 0.12
$t\bar{t}t\bar{t}$	0.02 ± 0.01	0.01 ± 0.01	0.7 ± 0.4	0.28 ± 0.15	0.34 ± 0.17	0.54 ± 0.28	–
Diboson	8.9 ± 2.9	2.6 ± 0.8	1.4 ± 0.5	0.48 ± 0.17	0.5 ± 0.3	0.7 ± 0.3	–
Rare	0.7 ± 0.4	0.29 ± 0.16	2.5 ± 1.3	0.9 ± 0.5	0.9 ± 0.5	1.0 ± 0.6	0.12 ± 0.07
Fake/non-prompt leptons	0.23 ± 0.23	0.15 ± 0.15	4.2 ± 3.1	0.5 ± 0.5	2.6 ± 2.2	2.3 ± 1.9	0.9 ± 0.7
Charge-flip	–	–	–	–	0.25 ± 0.04	0.25 ± 0.05	0.39 ± 0.08
Total Background	11.0 ± 3.0	3.3 ± 0.8	17 ± 4	3.9 ± 0.9	9.9 ± 2.9	9.8 ± 2.6	1.6 ± 0.8
Observed	9	3	20	4	14	13	1
S^{95}_{obs}	8.3	5.4	14.7	6.1	13.7	12.4	3.9
S^{95}_{exp}	$9.3^{+3.1}_{-2.3}$	$5.5^{+2.2}_{-1.5}$	$12.6^{+5.1}_{-3.4}$	$5.9^{+2.2}_{-1.8}$	$10.0^{+3.7}_{-2.6}$	$9.7^{+3.4}_{-2.6}$	$4.0^{+1.8}_{-0.3}$
σ_{vis} [fb]	0.23	0.15	0.41	0.17	0.38	0.34	0.11
p_0 (Z)	0.72 (–)	0.85 (–)	0.32 (0.5σ)	0.46 (0.1σ)	0.17 (1.0σ)	0.21 (0.8σ)	0.56 (–)

Signal Region	**Rpv2L1bH**	**Rpv2L0b**	**Rpv2L2bH**	**Rpv2L2bS**	**Rpv2L1bS**	**Rpv2L1bM**
$t\bar{t}+W/Z\gamma^*$	0.56 ± 0.14	0.14 ± 0.08	0.56 ± 0.15	6.5 ± 1.3	10.1 ± 1.7	1.4 ± 0.5
$t\bar{t}H$	0.07 ± 0.05	0.02 ± 0.02	0.12 ± 0.07	1.0 ± 0.5	1.9 ± 1.0	0.28 ± 0.15
$t\bar{t}t\bar{t}$	0.34 ± 0.17	0.01 ± 0.01	0.48 ± 0.24	1.6 ± 0.8	1.8 ± 0.9	0.53 ± 0.27
Diboson	0.14 ± 0.06	0.52 ± 0.21	0.04 ± 0.02	0.42 ± 0.16	1.7 ± 0.6	0.42 ± 0.15
Rare	0.29 ± 0.17	0.10 ± 0.06	0.19 ± 0.13	1.5 ± 0.8	2.4 ± 1.2	0.8 ± 0.4
Fake/non-prompt leptons	0.15 ± 0.15	0.18 ± 0.31	0.15 ± 0.15	8 ± 7	6 ± 6	1.3 ± 1.2
Charge-flip	0.02 ± 0.01	0.03 ± 0.02	0.03 ± 0.01	0.46 ± 0.08	0.74 ± 0.12	0.10 ± 0.02
Total Background	1.6 ± 0.4	1.0 ± 0.4	1.6 ± 0.5	19 ± 7	25 ± 7	4.8 ± 1.6
Observed	2	2	1	20	26	9
S^{95}_{obs}	4.8	5.2	3.9	17.5	18.1	11.4
S^{95}_{exp}	$4.1^{+1.9}_{-0.4}$	$4.0^{+1.7}_{-0.3}$	$4.1^{+1.8}_{-0.4}$	$16.8^{+5.2}_{-4.2}$	$17.2^{+5.9}_{-4.2}$	$7.3^{+2.5}_{-1.8}$
σ_{vis} [fb]	0.13	0.14	0.11	0.48	0.50	0.31
p_0 (Z)	0.33 (0.4σ)	0.19 (0.9σ)	0.55 (–)	0.48 (0.1σ)	0.44 (0.2σ)	0.07 (1.5σ)

Table 5: Numbers of events observed in the signal regions compared with background expectations. The "rare" category is defined in the text. Background categories shown as a "–" denote that they cannot contribute to a given region (e.g. charge flips in 3-lepton regions) or that their estimates are below 0.01. The 95% Confidence Level (CL) upper limits are shown on the observed and expected number of BSM events, S^{95}_{obs} and S^{95}_{exp} (as well as the $\pm 1\sigma$ excursions from this expectation), respectively. The 95% CL upper limits on the visible cross-section (σ_{vis}) is also given. Finally the p-values (p_0) give the probabilities of the observations being consistent with the estimated backgrounds. The number of equivalent Gaussian standard deviations (Z) are also shown when $p_0 < 0.5$.

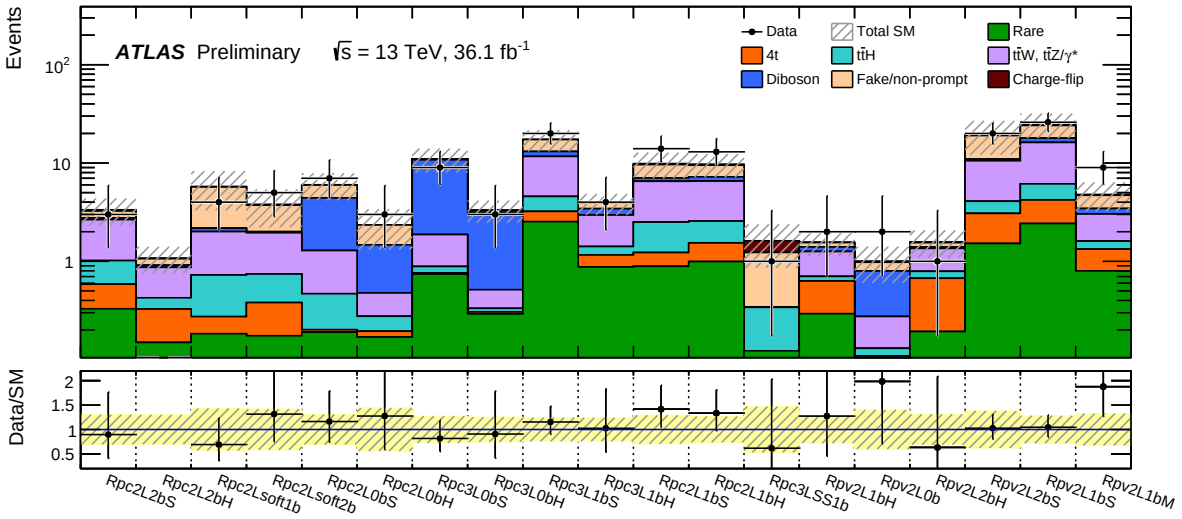

(a)

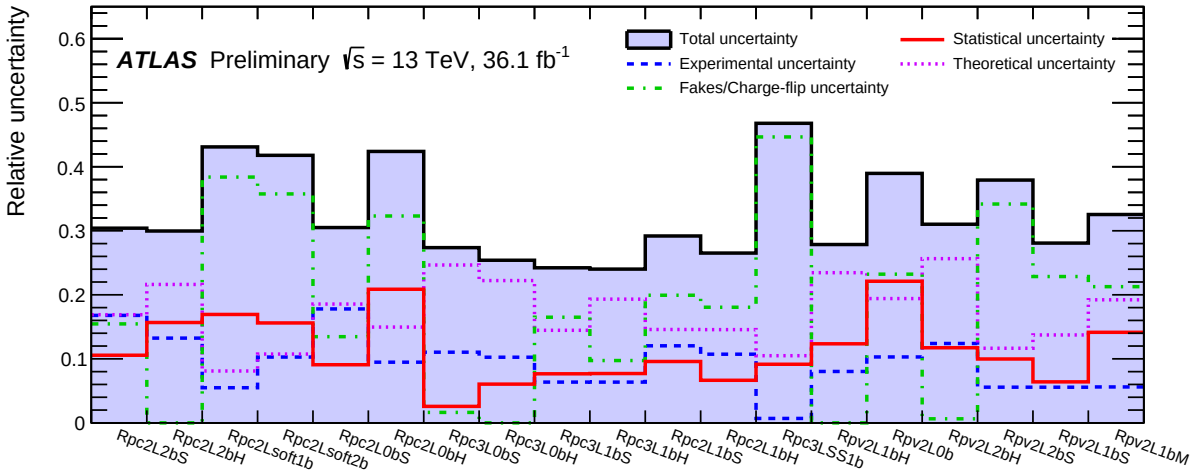

(b)

Figure 3: Comparison of the observed and expected event yields in each signal region (a) and relative uncertainties on the total background yield estimation (b). On the latter, "statistical uncertainty" corresponds to reducible and irreducible background statistical uncertainties. The background expectations correspond to those presented in Table 5 and the "rare" category is explained in the text.

in the benchmark scenarios of Figure 1. The HistFitter framework [93], which utilises a profile-likelihood-ratio test [94], is used to establish 95% confidence intervals using the CL_s prescription [95]. The likelihood is built as the product of a Poisson probability density function describing the observed number of events in the signal region and Gaussian distributions constraining the nuisance parameters associated with the systematic uncertainties whose widths correspond to the sizes of these uncertainties; Poisson distributions are used instead for MC simulation uncertainties. Correlations of a given nuisance parameter between the different sources of backgrounds and the signal are taken into account when relevant. The hypothesis

tests are performed for each of the signal regions, independently.

Table 5 presents 95% confidence level (CL) observed (expected) model-independent upper limits on the number of BSM events, S^{95}_{obs} (S^{95}_{exp}), that may contribute to the signal regions. Normalizing these by the integrated luminosity L of the data sample, they can be interpreted as upper limits on the visible BSM cross-section (σ_{vis}), defined as $\sigma_{\text{vis}} = \sigma_{\text{prod}} \times A \times \epsilon = S^{95}_{obs}/L$, where σ_{prod} is the production cross-section, A the acceptance and ϵ the reconstruction efficiency. The largest deviation between the data and background prediction corresponds to a 1.5 standard deviation excess in the Rpv2L1bM SR.

Exclusion limits at 95% CL are also set on the masses of the superpartners involved in the SUSY benchmark scenarios considered. Apart from the NUHM2 model, simplified models are used, corresponding to a single production mode and with 100% branching ratio to a specific decay chain, with the masses of the SUSY particles not involved in the process set to very high values. Figures 4, 5 and 6 show the exclusion limits on all the models considered in Figure 1 and the NUHM2 model. The assumptions on the decay chain considered for the different SUSY particles are stated above each figure. For each region of the signal parameter space, the SR with the best expected sensitivity is chosen.

For the RPC models, the limits set by this analysis are compared with the existing limits set by other ATLAS SUSY searches [23, 96]. For the models shown in Figure 4, the mass limits on gluinos and bottom squarks are increased by up to 400 GeV compared to the previous limits, reflecting the improvements in the signal region definitions as well as the increase in luminosity. Gluinos with masses up to 1.85 TeV are excluded in scenarios with a light $\tilde{\chi}^0_1$ in Figure 4(a). More generally, gluino masses below 1.57 TeV and bottom squarks with masses below 700 GeV are excluded for models with a massless LSP. The "compressed" regions, where SUSY particle masses are close-by, are also better covered and LSP masses up to 1200 and 250 GeV are excluded in the gluino and bottom squark pair-production models, respectively. Of particular interest is the observed exclusion of models producing gluino pairs with an off-shell top quark in the decay (Figure 1(b)), see Figure 4(a). In this case, models are excluded for mass differences between the gluino and neutralino of 220 GeV for a gluino mass below 1 TeV. The Rpc3LSS1b SR allows to exclude top squarks with masses below 700 GeV when the top squark decays to a top quark and a cascade of electroweakinos $\tilde{\chi}^0_2 \to \tilde{\chi}^\pm_1 W^\mp \to W^* W^\mp \tilde{\chi}^0_1$ (see Figure 4(e) for the conditions on the sparticle masses).

For the RPV models considering gluino pair production (Figure 5(a) – 5(d)), a generic exclusion of gluinos with masses below 1.3 TeV is obtained. Weaker exclusion limits are obtained for models considering pair production of $\tilde{d}_R$, which are typically around 500 GeV (Figure 5(e), 5(f)).

Finally, in the low fine-tuned NUHM2 model, the parameter $m_{1/2}$ is excluded below 615 GeV which corresponds to a gluino mass of 1500 GeV (Figure 6).

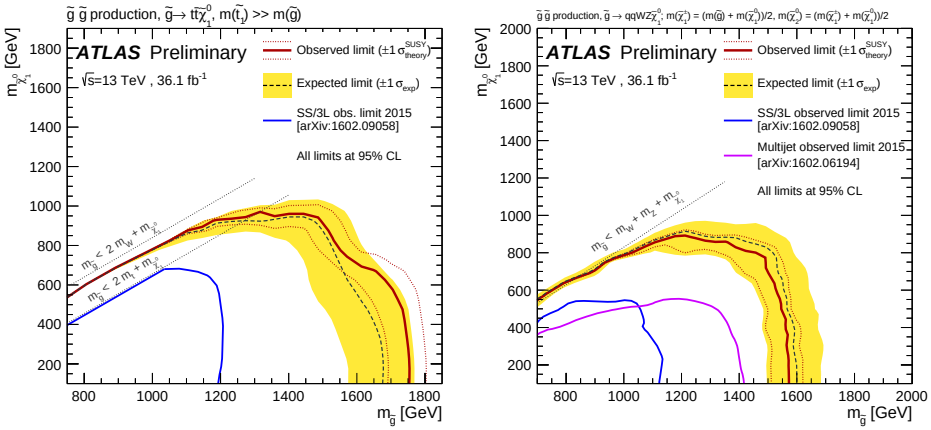

(a) Rpc2L2bS/H, Rpc2Lsoft1b/2b

(b) Rpc2L0bS, Rpc2L0bH

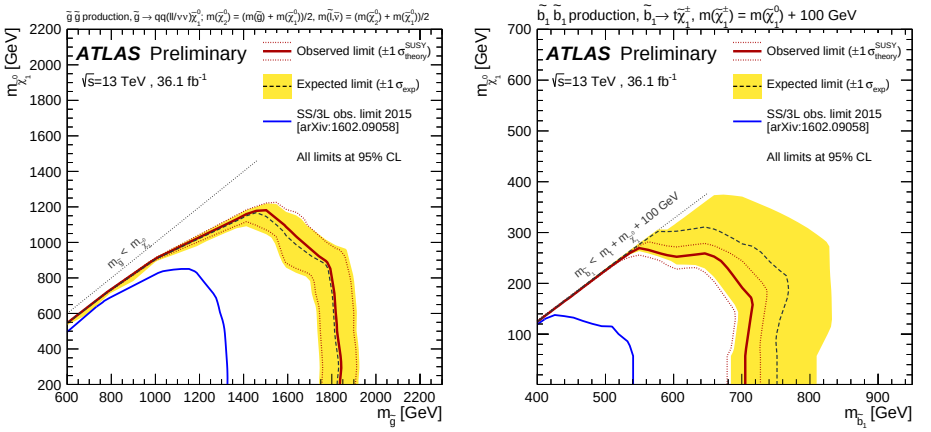

(c) Rpc3L0bS, Rpc3L0bH

(d) Rpc2L1bS, Rpc2L1bH

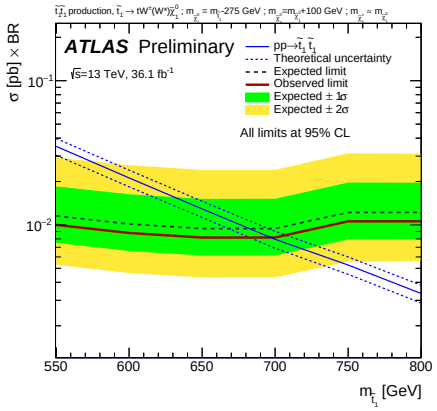

(e) Rpc3LSS1b

Figure 4: Observed and expected exclusion limits on the $\tilde{g}$, $\tilde{b}_1$, $\tilde{t}_1$and $\tilde{\chi}_1^0$ masses in the context of RPC SUSY scenarios with simplified mass spectra. The signal regions used to obtain the limits are specified in the subtitle of each scenario. All limits are computed at 95% CL. The dotted lines around the observed limit illustrate the change in the observed limit as the nominal signal cross-section is scaled up and down by the theoretical uncertainty. The contours of the band around the expected limit are the $\pm 1\sigma$ results ($\pm 2\sigma$ is also considered in Figure 4(e)), including all uncertainties except the theoretical ones on the signal cross-section. In Figures 4(a)–4(d), the grey diagonal lines indicate the kinematic limit for the decays in each specified scenario and results are compared with the observed limits obtained by previous ATLAS searches [23, 96].

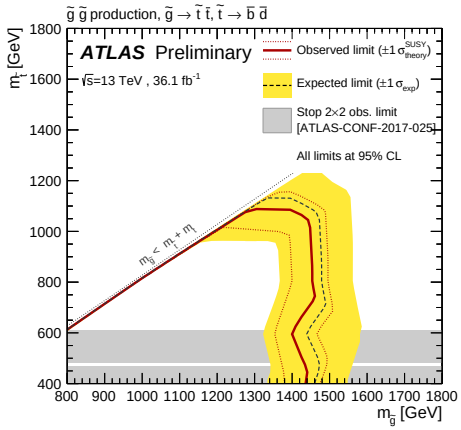

(a) Rpv2L1bH

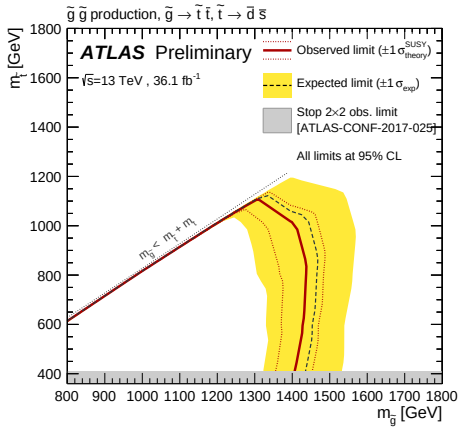

(b) Rpv2L1bH

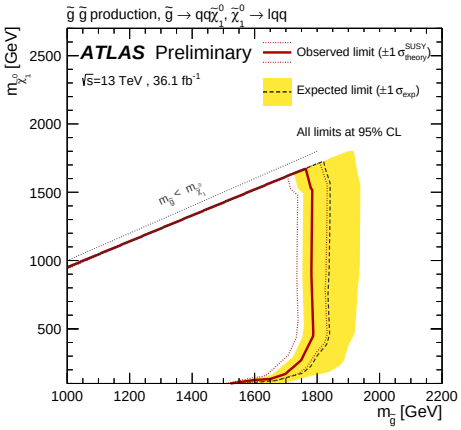

(c) Rpv2L0b

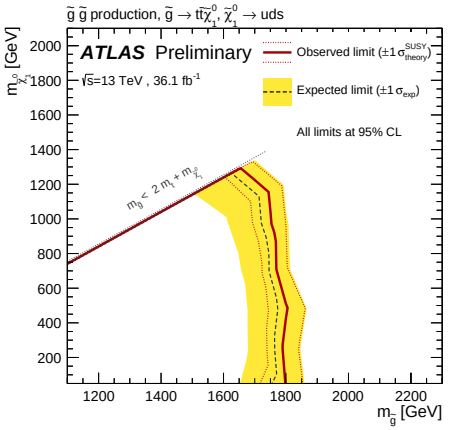

(d) Rpv2L2bH

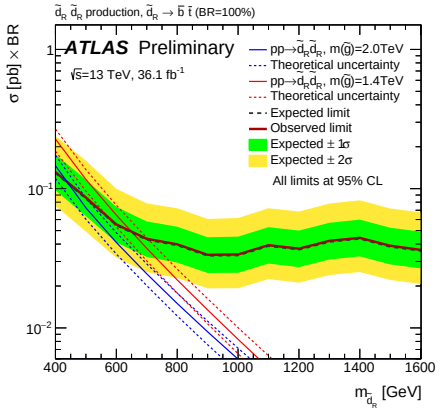

(e) Rpv2L2bS

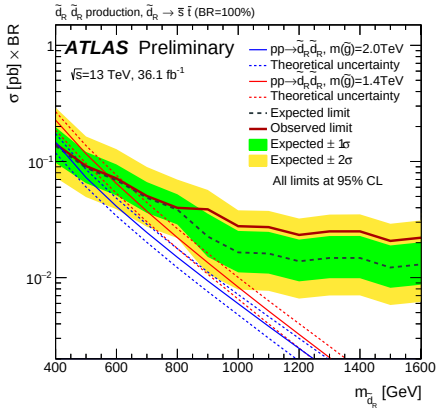

(f) Rpv2L1bS, Rpv2L1bM

Figure 5: Observed and expected exclusion limits on the $\tilde{g}$, $\tilde{t}_1$, $\tilde{d}_R$ and $\tilde{\chi}_1^0$ masses in the context of RPV SUSY scenarios with simplified mass spectra featuring $\tilde{g}\tilde{g}$ or $\tilde{d}_R\tilde{d}_R$ pair production with exclusive decay modes. The signal regions used to obtain the limits are specified in the subtitle of each scenario. All limits are computed at 95% CL. The dotted lines around the observed limit illustrate the change in the observed limit as the nominal signal cross-section is scaled up and down by the theoretical uncertainty. The contours of the band around the expected limit are the $\pm 1\sigma$ results, including all uncertainties except theoretical uncertainties on the signal cross-section ($\pm 2\sigma$ is also considered in Figures 5(e) and 5(f)). In Figures 5(a)–5(d), the grey diagonal lines indicate the kinematic limit for the decays in each specified scenario. For Figure 5(e) and 5(f), the region where the alternative decay channel $\tilde{d}_R \to \tilde{g}d$ is open, is considered for two different masses of gluinos.

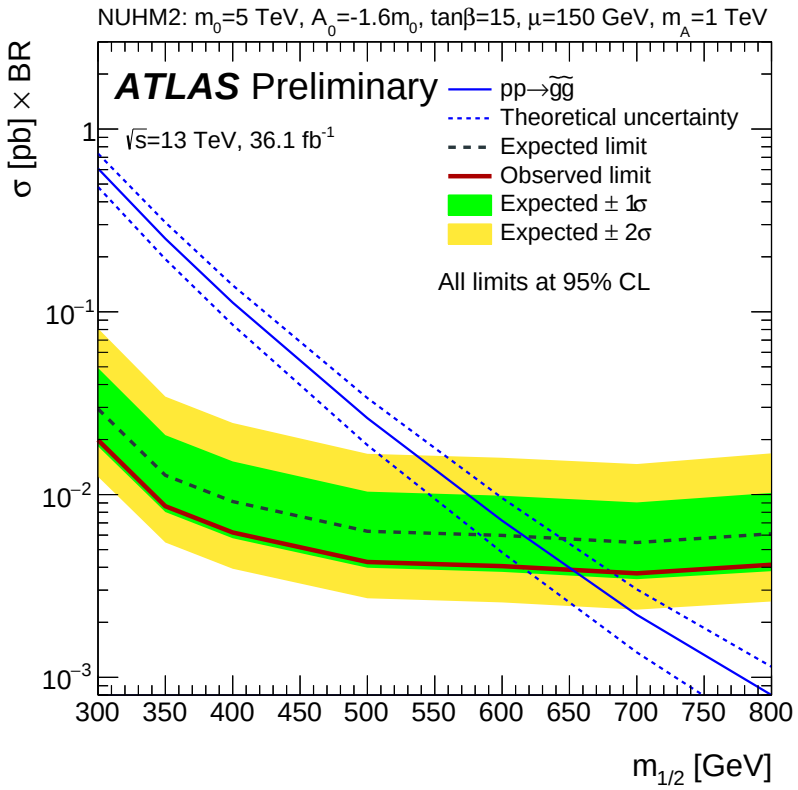

Figure 6: Observed and expected exclusion limits as a function of $m_{1/2}$ for the NUHM2 model [31, 32]. The signal region Rpc2L2bH is used to obtain the limits. The contours of the band around the expected limit are the $\pm 1\sigma$ results, including all uncertainties except theoretical uncertainties on the signal cross-section. The dotted lines around the observed limit illustrate the change in the observed limit as the nominal signal cross-section is scaled up and down by the theoretical uncertainty. The limits are computed at 95% CL.

7 Conclusion

A search for supersymmetry in events with two same-sign leptons or at least three leptons, multiple jets, b-jets and large $E_{\mathrm{T}}^{\mathrm{miss}}$ and/or large m_{eff} is presented. The analysis is performed with proton–proton collision data at $\sqrt{s} = 13$ TeV collected in 2015 and 2016 with the ATLAS detector at the Large Hadron Collider corresponding to an integrated luminosity of 36.1 fb^{-1}. With no significant excess over the Standard Model expectation observed, results are interpreted in the framework of simplified models featuring gluino and squark production in R-parity conserving and R-parity violating scenarios. Upper limits on particle masses are derived at 95% confidence level. In the $\tilde{g}\tilde{g}$ simplified RPC models considered, gluinos with masses up to 1.85 TeV are excluded in scenarios with a light $\tilde{\chi}_1^0$. RPC models with bottom squark masses below 700 GeV are also excluded in a $\tilde{b}_1\tilde{b}_1^*$ simplified model with $\tilde{b}_1 \to tW^-\tilde{\chi}_1^0$ and a light $\tilde{\chi}_1^0$. In RPV scenarios, masses of down squark-rights are probed up to $m_{\tilde{d}_R} \approx 500$ GeV. All models with gluino masses below 1.3 TeV are excluded, extending greatly the previous exclusion limits. Model independent limits on the cross-section of a possible signal contribution to the signal regions are set.

References

[1] Yu. A. Gol'fand and E. P. Likhtman,
Extension of the algebra of Poincaré group generators and violation of P invariance,
JETP Lett. **13** (1971) 323, [Pisma Zh. Eksp. Teor. Fiz.**13** (1971) 452].

[2] D. V. Volkov and V. P. Akulov, *Is the neutrino a Goldstone particle?*, Phys. Lett. B **46** (1973) 109.

[3] J. Wess and B. Zumino, *Supergauge transformations in four dimensions*,
Nucl. Phys. B **70** (1974) 39.

[4] J. Wess and B. Zumino, *Supergauge invariant extension of quantum electrodynamics*,
Nucl. Phys. B **78** (1974) 1.

[5] S. Ferrara and B. Zumino, *Supergauge invariant Yang-Mills theories*,
Nucl. Phys. B **79** (1974) 413.

[6] A. Salam and J. Strathdee, *Super-symmetry and non-Abelian gauges*, Phys. Lett. B **51** (1974) 353.

[7] S. P. Martin, *A Supersymmetry Primer*, Adv. Ser. Direct. High Energy Phys. **18** (1998) 1,
arXiv: hep-ph/9709356.

[8] P. Fayet, *Supersymmetry and weak, electromagnetic and strong interactions*,
Phys. Lett. B **64** (1976) 159.

[9] P. Fayet,
Spontaneously broken supersymmetric theories of weak, electromagnetic and strong interactions,
Phys. Lett. B **69** (1977) 489.

[10] G. R. Farrar and P. Fayet, *Phenomenology of the production, decay, and detection of new hadronic states associated with supersymmetry*, Phys. Lett. B **76** (1978) 575.

[11] H. Goldberg, *Constraint on the Photino Mass from Cosmology*,
Phys. Rev. Lett. **50** (1983) 1419, [Erratum: Phys. Rev. Lett. **103** (2009) 099905].

[12] J. Ellis et al., *Supersymmetric relics from the Big Bang*, Nucl. Phys. B **238** (1984) 453.

[13] N. Sakai, *Naturalness in Supersymmetric GUTS*, Z. Phys. C **11** (1981) 153.

[14] S. Dimopoulos, S. Raby and F. Wilczek, *Supersymmetry and the scale of unification*, Phys. Rev. D **24** (1981) 1681.

[15] L. E. Ibáñez and G. G. Ross, *Low-energy predictions in supersymmetric grand unified theories*, Phys. Lett. B **105** (1981) 439.

[16] S. Dimopoulos and H. Georgi, *Softly broken supersymmetry and SU(5)*, Nucl. Phys. B **193** (1981) 150.

[17] R. Barbieri and G. F. Giudice, *Upper bounds on supersymmetric particle masses*, Nucl. Phys. B **306** (1988) 63.

[18] B. de Carlos and J. A. Casas, *One loop analysis of the electroweak breaking in supersymmetric models and the fine tuning problem*, Phys. Lett. B **309** (1993) 320, arXiv: hep-ph/9303291.

[19] K. Inoue, A. Kakuto, H. Komatsu and S. Takeshita, *Aspects of Grand Unified Models with Softly Broken Supersymmetry*, Prog. Theor. Phys. **68** (1982) 927, [Erratum: Prog. Theor. Phys. **70** (1983) 330].

[20] J. Ellis and S. Rudaz, *Search for supersymmetry in toponium decays*, Phys. Lett. B **128** (1983) 248.

[21] C. Borschensky et al., *Squark and gluino production cross sections in pp collisions at $\sqrt{s}$ = 13, 14, 33 and 100 TeV*, Eur. Phys. J. C **74** (2014) 3174, arXiv: 1407.5066 [hep-ph].

[22] ATLAS Collaboration, *The ATLAS Experiment at the CERN Large Hadron Collider*, JINST **3** (2008) S08003.

[23] ATLAS Collaboration, *Search for supersymmetry at $\sqrt{s}$ = 13 TeV in final states with jets and two same-sign leptons or three leptons with the ATLAS detector*, Eur. Phys. J. C **76** (2016) 259, arXiv: 1602.09058 [hep-ex].

[24] CMS Collaboration, *Search for new physics in same-sign dilepton events in proton–proton collisions at $\sqrt{s}$ = 13 TeV*, Eur. Phys. J. C **76** (2016) 439, arXiv: 1605.03171 [hep-ex].

[25] CMS Collaboration, *Search for supersymmetry with multiple charged leptons in proton–proton collisions at $\sqrt{s}$ = 13 TeV*, Submitted to Eur. Phys. J. C (2017), arXiv: 1701.06940 [hep-ex].

[26] CMS Collaboration, *Search for physics beyond the standard model in events with two leptons of same sign, missing transverse momentum, and jets in proton–proton collisions at $\sqrt{s}$ = 13 TeV*, Submitted to Eur. Phys. J. C (2017), arXiv: 1704.07323 [hep-ex].

[27] J. Alwall, M.-P. Le, M. Lisanti and J. G. Wacker, *Searching for directly decaying gluinos at the Tevatron*, Phys. Lett. B **666** (2008) 34, arXiv: 0803.0019 [hep-ph].

[28] J. Alwall, P. C. Schuster and N. Toro, *Simplified models for a first characterization of new physics at the LHC*, Phys. Rev. D **79** (2009) 075020, arXiv: 0810.3921 [hep-ph].

[29] D. Alves, *Simplified models for LHC new physics searches*, J. Phys. G **39** (2012) 105005, ed. by N. Arkani-Hamed et al., arXiv: 1105.2838 [hep-ph].

[30] P. Huang, A. Ismail, I. Low and C. E. M. Wagner, *Same-sign dilepton excesses and light top squarks*, Phys. Rev. D **92** (2015) 075035, arXiv: 1507.01601 [hep-ph].

[31] J. Ellis, T. Falk, K. A. Olive and Y. Santoso,
Exploration of the MSSM with non-universal Higgs masses, Nucl. Phys. B **652** (2003) 259,
arXiv: hep-ph/0210205.

[32] J. Ellis, K. A. Olive and Y. Santoso,
The MSSM parameter space with non-universal Higgs masses, Phys. Lett. B **539** (2002) 107,
arXiv: hep-ph/0204192.

[33] E. Nikolidakis and C. Smith, *Minimal flavor violation, seesaw, and R-parity*,
Phys. Rev. D **77** (2008) 015021, arXiv: 0710.3129 [hep-ph].

[34] C. Smith, *Minimal flavor violation as an alternative to R-parity*,
Proceedings of the 34th International Conference on High Energy Physics (2008),
arXiv: 0809.3152 [hep-ph].

[35] C. Csáki, Y. Grossman and B. Heidenreich,
Minimal flavor violation supersymmetry: A natural theory for R-Parity violation,
Phys. Rev. D **85** (2012) 095009, arXiv: 1111.1239 [hep-ph].

[36] G. Durieux and C. Smith, *The same-sign top signature of R-parity violation*, JHEP **10** (2013) 068,
arXiv: 1307.1355 [hep-ph].

[37] J. Berger, M. Perelstein, M. Saelim and P. Tanedo,
The same-sign dilepton signature of RPV/MFV SUSY, JHEP **04** (2013) 077,
arXiv: 1302.2146 [hep-ph].

[38] ATLAS Collaboration, *ATLAS Insertable B-Layer Technical Design Report*, ATLAS-TDR-19,
2010, URL: https://cds.cern.ch/record/1291633,
ATLAS Insertable B-Layer Technical Design Report Addendum, ATLAS-TDR-19-ADD-1, 2012,
URL: https://cds.cern.ch/record/1451888.

[39] ATLAS Collaboration, *Performance of the ATLAS Trigger System in 2015*,
Submited to Eur. Phys. J. C (2016), arXiv: 1611.09661 [hep-ex].

[40] ATLAS Collaboration,
Luminosity determination in pp collisions at $\sqrt{s} = 8$ TeV using the ATLAS detector at the LHC,
Eur. Phys. J. C **76** (2016) 653, arXiv: 1608.03953 [hep-ex].

[41] ATLAS Collaboration, *The ATLAS simulation infrastructure*, Eur. Phys. J. C **70** (2010) 823,
arXiv: 1005.4568 [physics.ins-det].

[42] S. Agostinelli et al., *GEANT4: A simulation toolkit*, Nucl. Instrum. Meth. A **506** (2003) 250.

[43] ATLAS Collaboration,
The simulation principle and performance of the ATLAS fast calorimeter simulation FastCaloSim,
ATL-PHYS-PUB-2010-013, 2010, URL: https://cds.cern.ch/record/1300517.

[44] T. Sjöstrand, S. Mrenna and P. Skands, *A brief introduction to PYTHIA 8.1*,
Comput. Phys. Commun. **178** (2008) 852, arXiv: 0710.3820 [hep-ph].

[45] ATLAS Collaboration, *Summary of ATLAS Pythia 8 tunes*, ATL-PHYS-PUB-2012-003, 2012,
URL: https://cds.cern.ch/record/1474107.

[46] A. D. Martin, W. J. Stirling, R. S. Thorne and G. Watt, *Parton distributions for the LHC*,
Eur. Phys. J. C **63** (2009) 189, arXiv: 0901.0002 [hep-ph].

[47] D. J. Lange, *The EvtGen particle decay simulation package*,
Nucl. Instrum. Meth. A **462** (2001) 152.

[48] J. Alwall et al., *The automated computation of tree-level and next-to-leading order differential cross sections, and their matching to parton shower simulations*, JHEP **07** (2014) 079, arXiv: 1405.0301 [hep-ph].

[49] R. D. Ball et al., *Parton distributions with LHC data*, Nucl. Phys. B **867** (2013) 244, arXiv: 1207.1303 [hep-ph].

[50] ATLAS Collaboration, *ATLAS Pythia 8 tunes to* 7 *TeV data*, ATL-PHYS-PUB-2014-021, 2014, URL: https://cds.cern.ch/record/1966419.

[51] G. Corcella et al., *HERWIG 6: an event generator for hadron emission reactions with interfering gluons (including supersymmetric processes)*, JHEP **01** (2001) 010, arXiv: hep-ph/0011363.

[52] W. Beenakker, R. Höpker, M. Spira and P. Zerwas, *Squark and gluino production at hadron colliders*, Nucl. Phys. B **492** (1997) 51, arXiv: hep-ph/9610490.

[53] A. Kulesza and L. Motyka, *Threshold Resummation for Squark-Antisquark and Gluino-Pair Production at the LHC*, Phys. Rev. Lett. **102** (2009) 111802, arXiv: 0807.2405 [hep-ph].

[54] A. Kulesza and L. Motyka, *Soft gluon resummation for the production of gluino-gluino and squark-antisquark pairs at the LHC*, Phys. Rev. D **80** (2009) 095004, arXiv: 0905.4749 [hep-ph].

[55] W. Beenakker et al., *Soft-gluon resummation for squark and gluino hadroproduction*, JHEP **12** (2009) 041, arXiv: 0909.4418 [hep-ph].

[56] W. Beenakker et al., *Squark and gluino hadroproduction*, Int. J. Mod. Phys. A **26** (2011) 2637, arXiv: 1105.1110 [hep-ph].

[57] M. Krämer et al., *Supersymmetry production cross sections in pp collisions at* $\sqrt{s} = 7$ *TeV*, (2012), arXiv: 1206.2892 [hep-ph].

[58] J. Pumplin et al., *New Generation of Parton Distributions with Uncertainties from Global QCD Analysis*, JHEP **07** (2002) 012, arXiv: hep-ph/0201195.

[59] S. Gieseke, C. Röhr and A. Siodmok, *Colour reconnections in Herwig++*, Eur. Phys. J. C **72** (2012) 2225, arXiv: 1206.0041 [hep-ph].

[60] D. de Florian et al., *Handbook of LHC Higgs cross sections: 4. Deciphering the nature of the Higgs sector*, (2016), arXiv: 1610.07922 [hep-ph].

[61] T. Gleisberg et al., *Event generation with SHERPA 1.1*, JHEP **02** (2009) 007, arXiv: 0811.4622 [hep-ph].

[62] ATLAS Collaboration, *Multi-boson simulation for* 13 *TeV ATLAS analyses*, ATL-PHYS-PUB-2016-002, 2016, URL: https://cds.cern.ch/record/2119986.

[63] H.-L. Lai et al., *New parton distributions for collider physics*, Phys. Rev. D **82** (2010) 074024, arXiv: 1007.2241 [hep-ph].

[64] LHC Higgs Cross Section Working Group, *Handbook of LHC Higgs cross sections: 2. Differential distributions*, (2012), arXiv: 1201.3084 [hep-ph].

[65] L. Lönnblad and S. Prestel, *Matching tree-level matrix elements with interleaved showers*, JHEP **03** (2012) 019, arXiv: 1109.4829 [hep-ph].

[66] W. Beenakker, R. Höpker and M. Spira, *PROSPINO: A Program for the production of supersymmetric particles in next-to-leading order QCD*, (1996), arXiv: hep-ph/9611232.

[67] ATLAS Collaboration,
Modelling of the $t\bar{t}H$ and $t\bar{t}V$ ($V = W, Z$) processes for $\sqrt{s} = 13$ TeV ATLAS analyses,
ATL-PHYS-PUB-2016-005, 2016, URL: https://cds.cern.ch/record/2120826.

[68] S. Frixione et al.,
Electroweak and QCD corrections to top-pair hadroproduction in association with heavy bosons, JHEP **06** (2015) 184, arXiv: 1504.03446 [hep-ph].

[69] ATLAS Collaboration,
Vertex Reconstruction Performance of the ATLAS Detector at $\sqrt{s} = 13$ TeV,
ATL-PHYS-PUB-2015-026, 2015, URL: https://cds.cern.ch/record/2037717.

[70] ATLAS Collaboration, *Electron efficiency measurements with the ATLAS detector using the 2015 LHC proton–proton collision data*, ATLAS-CONF-2016-024, 2016,
URL: https://cds.cern.ch/record/2157687.

[71] ATLAS Collaboration, *Muon reconstruction performance of the ATLAS detector in proton–proton collision data at $\sqrt{s}$ =13 TeV*, Eur. Phys. J. C **76** (2016) 292, arXiv: 1603.05598 [hep-ex].

[72] M. Cacciari, G. P. Salam and G. Soyez, *The anti-k_t jet clustering algorithm*, JHEP **04** (2008) 063, arXiv: 0802.1189 [hep-ph].

[73] ATLAS Collaboration,
Topological cell clustering in the ATLAS calorimeters and its performance in LHC Run 1, (2016), arXiv: 1603.02934 [hep-ex].

[74] M. Cacciari and G. P. Salam, *Pileup subtraction using jet areas*, Phys. Lett. B **659** (2008) 119, arXiv: 0707.1378 [hep-ph].

[75] ATLAS Collaboration, *Jet energy scale measurements and their systematic uncertainties in proton–proton collisions at $\sqrt{s} = 13$ TeV with the ATLAS detector*,
Submitted to Phys. Rev. D (2017), arXiv: 1703.09665 [hep-ex].

[76] ATLAS Collaboration, *Tagging and suppression of pileup jets with the ATLAS detector*,
ATLAS-CONF-2014-018, 2014, URL: https://cds.cern.ch/record/1700870.

[77] ATLAS Collaboration, *Performance of b-jet identification in the ATLAS experiment*,
JINST **11** (2016) P04008, arXiv: 1512.01094 [hep-ex].

[78] ATLAS Collaboration, *Expected performance of the ATLAS b-tagging algorithms in Run-2*,
ATL-PHYS-PUB-2015-022, 2015, URL: https://cds.cern.ch/record/2037697.

[79] ATLAS Collaboration, *Optimisation of the ATLAS b-tagging performance for the 2016 LHC Run*,
ATL-PHYS-PUB-2016-012, 2016, URL: https://cds.cern.ch/record/2160731.

[80] ATLAS Collaboration, *Electron efficiency measurements with the ATLAS detector using 2012 LHC proton–proton collision data*, Eur. Phys. J. C **77** (2017) 195, arXiv: 1612.01456 [hep-ex].

[81] ATLAS Collaboration, *Measurement of the photon identification efficiencies with the ATLAS detector using LHC Run-1 data*, Eur. Phys. J. C **76** (2016) 666, arXiv: 1606.01813 [hep-ex].

[82] ATLAS Collaboration, *Performance of missing transverse momentum reconstruction with the ATLAS detector in the first proton–proton collisions at* $\sqrt{s}$ = 13 *TeV*, ATL-PHYS-PUB-2015-027, 2015, URL: https://cds.cern.ch/record/2037904.

[83] ATLAS Collaboration, *Expected performance of missing transverse momentum reconstruction for the ATLAS detector at* $\sqrt{s}$ = 13 *TeV*, ATL-PHYS-PUB-2015-023, 2015, URL: https://cds.cern.ch/record/2037700.

[84] ATLAS Collaboration, *Characterisation and mitigation of beam-induced backgrounds observed in the ATLAS detector during the 2011 proton–proton run*, JINST **8** (2013) P07004, arXiv: 1303.0223 [hep-ex].

[85] ATLAS Collaboration, *Jet energy measurement and its systematic uncertainty in proton–proton collisions at* $\sqrt{s}$ = 7 *TeV with the ATLAS detector*, Eur. Phys. J. C **75** (2015) 17, arXiv: 1406.0076 [hep-ex].

[86] ATLAS Collaboration, *Search for supersymmetry at* $\sqrt{s}$*=8 TeV in final states with jets and two same-sign leptons or three leptons with the ATLAS detector*, JHEP **06** (2014) 035, arXiv: 1404.2500 [hep-ex].

[87] ATLAS Collaboration, *Search for supersymmetry using events with three leptons, multiple jets, and missing transverse momentum in* 13.0 fb^{-1} *of pp collisions with the ATLAS detector at* $\sqrt{s}$ = 8 *TeV*, ATLAS-CONF-2012-151, 2012, URL: https://cds.cern.ch/record/1493490.

[88] P. Nason, *A new method for combining NLO QCD with shower Monte Carlo algorithms*, JHEP **11** (2004) 040, arXiv: hep-ph/0409146.

[89] S. Frixione, P. Nason and C. Oleari, *Matching NLO QCD computations with parton shower simulations: the POWHEG method*, JHEP **11** (2007) 070, arXiv: 0709.2092 [hep-ph].

[90] S. Alioli, P. Nason, C. Oleari and E. Re, *A general framework for implementing NLO calculations in shower Monte Carlo programs: the POWHEG BOX*, JHEP **06** (2010) 043, arXiv: 1002.2581 [hep-ph].

[91] J. M. Campbell, R. K. Ellis, P. Nason and E. Re, *Top-pair production and decay at NLO matched with parton showers*, JHEP **04** (2015) 114, arXiv: 1412.1828 [hep-ph].

[92] T. Sjöstrand, S. Mrenna and P. Skands, *PYTHIA 6.4 physics and manual*, JHEP **05** (2006) 026, arXiv: hep-ph/0603175.

[93] M. Baak et al., *HistFitter software framework for statistical data analysis*, Eur. Phys. J. C **75** (2015) 153, arXiv: 1410.1280 [hep-ex].

[94] G. Cowan, K. Cranmer, E. Gross and O. Vitells, *Asymptotic formulae for likelihood-based tests of new physics*, Eur. Phys. J. C **71** (2011) 1554, [Erratum: Eur. Phys. J. C **73** (2013) 2501], arXiv: 1007.1727 [physics.data-an].

[95] A. L. Read, *Presentation of search results: The CL(s) technique*, J. Phys. G **28** (2002) 2693, [,11(2002)].

[96] ATLAS Collaboration, *Search for new phenomena in final states with large jet multiplicities and missing transverse momentum with ATLAS using* $\sqrt{s}$ *= 13 TeV proton–proton collisions*, Phys. Lett. B **757** (2016) 334, arXiv: 1602.06194 [hep-ex].